**Title**

# Synaptic plasticity in the medial preoptic area of male mice encodes social experiences with female and regulates behavior toward young

Kazuki Ito[1], Keiichiro Sato[1], Yousuke Tsuneoka[2,3], Takashi Maejima[4], Hiroyuki Okuno[5], Yumi Hamasaki[1], Shunsaku Murakawa[1], Chihiro Yoshihara[2,6], Sayaka Shindo[2], Haruka Uki[1], Stefan Herlitze[7], Masahide Seki[8], Yutaka Suzuki[8], Takeshi Sakurai[9], Kumi O Kuroda[2,6], Masabumi Minami[1], Taiju Amano[1,2]*

[1] Department of Pharmacology, Graduate School of Pharmaceutical Sciences, Hokkaido University, 060-0812, Japan

[2] Laboratory for Affiliative Social Behavior, RIKEN Center for Brain Science, 351-0198, Japan

[3] Department of Anatomy, School of Medicine, Toho University, 143-8540, Japan

[4] Department of Integrative Neurophysiology, Graduate School of Medical Sciences, Kanazawa University, 920-8640, Japan

[5] Laboratory of Biochemistry and Molecular Biology, Graduate School of Medical and Dental Sciences, Kagoshima University, Kagoshima, 890-8520, Japan

[6] Dept. of Life Science and Technology, Tokyo Institute of Technology

[7] Department of General Zoology and Neurobiology, ND7/31, Ruhr-University Bochum, 44780, Germany

[8] Department of Computational Biology and Medical Sciences, Graduate School of Frontier Sciences, The University of Tokyo, 277-8562, Japan

[9] Faculty of Medicine/International Institute for Integrative Sleep Medicine (IIIS), University of Tsukuba, 305-8575, Japan

* **Correspondence to**: Taiju Amano, Department of Pharmacology, Graduate School of Pharmaceutical Sciences, Hokkaido University, Kita 12, Nishi 6, Kita-ku, Sapporo Hokkaido 060-0812, Japan Tel: +81-11-706-3246, Fax: +81-11-706-4987, E-mail: tamano@pharm.hokudai.ac.jp

**Keywords**:

paternal behavior, infanticide, aggression, social behavior, medial preoptic area, bed nucleus of the stria terminalis, electrophysiology

**Summary**

A dramatic shift from aggressive infanticidal to paternal social behaviors is an essential event for males after mating. While the central part of the medial preoptic area (cMPOA) has been shown to critically mediate the paternal behaviors in mice, how this brain region becomes activated by mating and subsequent interaction with pups has not been investigated. Here, we demonstrate that the reduction in inhibitory synaptic strength towards the cMPOA provided by posteriordorsal medial amygdala (MePD) neurons is a key event for the post-mating behavioral shift in males. Consistent with this, we found optogenetic disinhibition of $Me^{Cartpt}$ to the cMPOA synapses reduces male aggression towards pups. We further provide evidence that the cMPOA of paternal mice mediated pup-induced neural plastic changes in the bed nucleus of the stria terminalis. These findings provide possible function of cMPOA neural circuits required for the reception to young in male mice.

**Introduction**

Reproductive behavior in male includes courting, mating and parental behavior. Polygynous male mammals, which form reproductive groups with one male and multiple females, often show aggressive behavior toward un-familiar infant conspecifics[1-5]. Infanticide of non-offspring young is commonly believed to improve reproductive success by achieving a shorter inter-birth interval for

females, a situation more favorable to breeding lower competition for resources, and the avoidance of misdirected paternal investment[3,6]. After mating, however, the same male gradually stops committing infanticide and becomes paternal, even toward non-biological offspring[5]. This behavioral transition from infanticide to paternal care in C57BL/6 male mice is shown to require not only the experience of ejaculation but also cohabitation with the pregnant female[7,8]. The exact neural mechanisms governing this behavioral transition through social experiences with female and infant remained unknown.

The medial preoptic area (MPOA) has been identified as one of the most important brain regions regulating parental behavior[9]. Within the MPOA, the central part (cMPOA), located ventral to the cluster of magnocellular oxytocin neurons (the anterior commissural nucleus), appears to play a pivotal role in parental behavior because bilateral cMPOA lesions abolished this behavior and promoted infanticide in both maternal and paternal mice[10,11]. Likewise, optogenetic activation of the MPOA in virgin male mice delayed infanticidal behavior[11,12]. However, the neural circuit mechanisms that control the MPOA neuronal activities was not clear. Previously, we reported that behavioral mode transition from infanticide to parental was initiated by lesions of vomeronasal organ (VNO), which transmits olfactory information to the accessory olfactory bulb[8]. Similar results were obtained in the experiment using genetically mutated mice with impaired vomeronasal signaling[12]. Tracing studies using classical retrograde tracer or rabies virus indicate that sensory information from accessary olfactory system is mediated by the bed nucleus of the stria terminalis (BST) and the medial amygdala (Me) and is

transmitted to the MPOA[13-15]. It is reported that aggressive behavior toward pup is elicited by activation of GABAergic Me[16,17].

The present study evaluates the efficacy of synaptic transmission from the Me to putative *Galanin*-positive cMPOA neurons from three groups: (i) males that experienced mating and pup exposure, (ii) males that experienced mating but had not pup exposure, and (iii) virgin males. We observed that inhibitory inputs from the Me to cMPOA were suppressed ahead of pup delivery, leading to cMPOA disinhibition. Optogenetic inhibition of Me–cMPOA synapses significantly reduced the proportion of mice showing aggressive behavior toward pups. Furthermore, we found paternal experiences increased synaptic inhibition in the rhomboid nucleus of the bed nucleus of the stria terminalis (BSTrh), one of a downstream structure of the MPOA[11]. Together, findings indicate that alterations in plasticity at Me–cMPOA synapses occur as a result of social experience with a female partner, which may function to prime a shift in behavioral response toward pups. This is followed by paternal experience with pups inducing changes in BSTrh.

## Results

### Sensitivity to GABAergic synaptic inputs from the Me to the cMPOA are suppressed by mating experience and cohabitation with a late gestational female

To map the projections from the Me to cMPOA, we took advantage of the high expression of the peptide, cocaine and amphetamine regulated transcript (Cart), in the subpopulation of posterior-

dorsal Me (MePD) neurons[18,19]. Within the Me, clusters of Cart-positive neurons were clearly visualized in the MePD by immunostaining with an anti-Cart antibody (Figure S1A). We infused biotin dextran amine (BDA), an anterograde neuron tracer, into the Cart-positive area of the Me (Figure 1A and Figure B) and observed a projection to the cMPOA (Figure 1C and Figure S1B). The cMPOA is located ventral to the anterior commissural nucleus, which contains magnocellular oxytocin neurons and thus could be visualized using an antibody for the oxytocin-associated protein neurophysin I (NPI)[10]. In contrast to the Cart-positive area of the Me, the Cart-negative area did not send a dense projection to the cMPOA regardless of tiny BDA leak in Cart-positive area of the Me (Figure S1C-F).

To address the cell-type in the cMPOA, the cMPOA neurons were manually collected using a glass pipette and RNA-seq analysis was performed to evaluate mRNA expression levels. A six cell-sample was combined and represented as data for one mouse. Here, we established three age-matched experimental groups of male mice with different levels of paternal experience: 1) males each co-housed with one female for mating, gestation, delivery, and remaining with the pups for the first 3 postnatal days (paternal group), 2) males each co-housed with one female mating partner until late gestation without exposure to pups (fathers in gestation experience; FGE group[20]), and 3) virgin male mice. Table S1 lists the differentially expressed genes (DEGs) in cMPOA neurons among virgin (V), FGE (F), and paternal (P) mice. Further, we evaluated the expression levels of 21 representative genes levels previously reported in activated MPOA neurons during social behavior[21]

to explore the recorded neuron's cell-type in this study and found no difference in their expression levels among the groups (Figure 1D). Among all samples, expression level of *Galanin* (*Gal*) was the highest. Previous studies have shown that the activation of Gal-Cre labeled MPOA neurons can block infanticide in virgin male mice[12,14]. We visualized *Galanin* mRNA-positive neurons with Alexa647 using *in situ* hybridization chain reaction (HCR). We observed a banded *Galanin*-expressing region extending ventrally from the posterior part of the anterior commissure (AC) and covering the cMPOA region (Figure 1E). Biocytin injected neurons during patch clamp recording were visualized by reacting it with streptavidin conjugated to fluorescein isothiocyanate (FITC). We observed that 85.0% (34 in 40 cells) of the recorded neurons were positive for *Galanin* mRNA co-staining (Figure 1F and 1G). Meanwhile, Esr1, another marker gene in the MPOA region related to parental behavior[21-23], was moderately detected among the groups (Figure 1D). Histological analysis revealed that ERα-positive neurons (protein from the Esr1 translation) covered the cMPOA region, which is locaged ventrally to NPI-positive neuronal clusters (Figure 1H). Compared with *Galanin*, the ERα-positive neurons were broadly expressed in MPOA (Figure 1I). Further, 50% of patch clamp recorded neurons (7 of 14 cells) were ERα positive (Figure 1J and 1K).

Next, to examine if social experience-dependent plastic changes in the cMPOA underlie the shift from infanticidal to paternal behavior, we performed whole-cell patch clamp recordings of cMPOA neurons from paternal, FGE, and virgin group mice to compare the synaptic responses. There were no significant differences in passive membrane properties of cMPOA neurons among the

groups (Table S2 and S3). The projections including those from Cart-positive Me to the cMPOA were electrically stimulated (Figure 1L), and the cell types of the recorded neurons were confirmed by post hoc *in situ* hybridization staining. The average evoked inhibitory postsynaptic potential amplitude was significantly smaller in the FGE group *Galanin*-positive cMPOA neurons compared with the virgin group *Galanin*-positive cMPOA neurons (Figure 1M). A similar trend was observed in the experiments in the blind targeted cMPOA neurons from the virgin and FGE groups (Figure S2A). Considering that a high percentage of *Galanin*-positive neurons were targeted in the cMPOA (Figure 1G), we considered that we were, in most cases, recording from *Galanin*-positive neurons. Consequently, cell types are not discussed for each of the following experiments. Similar to FGE mice, paternal mice showed a significant level of decreased eIPSP amplitude in the cMPOA compared with the virgin mice (Figure 1N). We also addressed the effects of pregnant female exposure alone (i.e., without the experience of copulation and delivery) on virgin males (virgin male with late gestation; VMLG group, Figure S2B) or sexual experience without staying until late gestation of female partner (male with mating experience; MME, Figure S2D). As a result, eIPSP amplitude in the cMPOA in VMLG and MME mice were not changed (Figure S2C and S2E), suggesting that either mating experience or cohabitation with a late gestational female was not enough to reduce eIPSP amplitude in the cMPOA. To test the postsynaptic factors contribution to plastic changes in paternal mice, a G-protein signaling blocker GDPβS was intracellularly infused. The decreased eIPSP amplitude in the paternal group mice's cMPOA was reversed by GDPβS

intracellular infusion (Figure 1O). Collectively, these data suggested that mating and cohabitation with a female, but not experience with pup, activates intracellular signals inducing disinhibition in the cMPOA, which densely include *Galanin*-positive neurons.

Average evoked excitatory postsynaptic potentials (eEPSPs) amplitudes did not differ between the groups (Figure 1P).

**Me$^{Cartpt}$ neuron projections to cMPOA neurons are modified by female exposure alone**

To directly test if the eIPSP decrease observed in the cMPOA of FGE group mice is mediated by input from Me neurons, we utilized Cartpt (which encodes Cart)-Cre mice. Cartpt-Cre × Ai9 reporter mice showed that 21.2% of NeuN-positive neurons in MePD were Cartpt (tdTomato) positive (Figure 2A). We first infused an AAV vector encoding Cre-dependent eYFP into the Me of Cartpt-Cre mice for pathway identification (Figure 2B). Indeed, we observed a clear Cre-dependent eYFP expression in Me$^{Cartpt}$ neurons and eYFP-labeled projections into the cMPOA (Figure 2C and 2D), consistent with the tracer study (Figure 1B and 1C). Next, we infused an AAV vector to express blue light-sensitive channelrhodopsin, ChR2(H134R) in Me$^{Cartpt}$ neurons and performed whole-cell patch clamp recordings from cMPOA neurons in slices prepared from these mice. Application of blue light to brain slices including the cMPOA depolarized the synaptic terminals derived from Me$^{Cartpt}$ neurons and induced both excitatory and inhibitory synaptic currents in cMPOA neurons (Figure 2E and 2F), so we evaluated social experience-dependent synaptic changes at both excitatory and

inhibitory pathways. At the recording potential (−60 mV), glutamatergic and GABAergic ionotropic receptor currents should flow in the opposite direction. Thus, glutamatergic and GABAergic predominance can be distinguished by the net change in membrane current. Because of the abundance of GABAergic neurons in the MePD[13], including retrogradely labeled cMPOA projecting MePD neurons (Figure S3), we chose an experimental protocol that emphasized the EPSC amplitude. The driving force for EPSC and IPSC, calculated by subtraction of the recording potential (−60 mV) and reversal potential (−1 mV for EPSC, −87 mV for IPSC calculated by Nernst equation), were about 59 mV and 27 mV, respectively. Under this experimental protocol, we counted cMPOA neurons expressing predominantly blue light-induced EPSCs or IPSCs by the net membrane current change. Whereas 83.3% of cMPOA neurons were IPSC-dominant in virgin male mice, only 21.4% were IPSC-dominant in FGE males (Figure 2G). In accordance with the electrically evoked responses (Figure 1O), intracellular perfusion of a G-protein signaling blocker GDPβS into the cMPOA neurons reversed the ratio of IPSC- dominant neurons in FGE males to the level of virgin males. As expected, control group mice expressing only eYFP did not show light-evoked synaptic responses (Figure 2G). The data presented so far suggest that experiencing mating and cohousing with a pregnant female impaired GABAergic synaptic transmission from $Me^{Cartpt}$ into the cMPOA.

**Optogenetic inhibition of Me-to-cMPOA inputs change the spontaneous synaptic activity**

184 To examine whether inhibition of $Me^{Cartpt}$ terminals in the cMPOA modulate neural and/or
185 synaptic activity, we attempted to specifically silence these synapses. For this, we infused an AAV
186 vector encoding vertebrate long-wavelength opsin (vLWO)[24,25] bilaterally into the Me of virgin
187 Cartpt-Cre mice to suppress $Me^{Cartpt}$ inputs (Figure 3A). To confirm the inhibitory effects of vLWO,
188 we performed whole-cell patch clamp recordings from $Me^{Cartpt}$ neurons expressing vLWO-eGFP.
189 Application of green light hyperpolarized $Me^{Cartpt}$ neurons (Figure 3B and 3C) but did not in the
190 control group (Figure 3D and 3E).

191 Next, we infused an AAV vector encoding ChR2 and vLWO into the Me of virgin Cartpt-Cre
192 mice to confirm the inhibitory effects of vLWO at the synaptic terminal (Figure 3F and 3G). After
193 more than 4 weeks, brain slices were prepared and recorded from cMPOA neurons. Green light
194 could affect ChR2 and therefore instead of using green light as above, red light was used to
195 stimulate the vLWO. The amplitude of blue light induced IPSC was significantly reduced by vLWO
196 activation (Figure 3H and 3I). Furthermore, the suppressed synaptic inputs from the $Me^{Cartpt}$ to the
197 MPOA could result not only in reduced direct synaptic transmission but also in more frequent
198 inhibitory synaptic currents by disinhibition of surrounding interneurons. To address this
199 hypothesis, we observed spontaneous IPSCs (sIPSC) in each cMPOA neuron before and after the
200 suppression of inputs from the $Me^{Cartpt}$ via vLWO activation (Figure 3J-L). Within 25 recorded
201 neurons, sIPSC frequency was increased more than 10% in 13 neurons and reduced more than 10%
202 in 1 neuron. The averaged frequency of the sIPSC in cMPOA was significantly increased (Figure 3L).

The application of tetorodotoxin (TTX) blocked the effects of vLWO activation (Figure 3M and 3N). These data suggest that inhibition of the $Me^{Cartpt}$ inputs to the MPOA could modify the activity of each neuron in the cMPOA by acting on inter-neuronal network.

**In vivo optogenetic inhibition of Me-cMPOA inputs suppresses infanticidal behavior**

We previously demonstrated that Me neurons in infanticidal virgin males are highly activated and express c-Fos protein following exposure to donor pups contained in wire mesh ball[8]. Consistent with those results, in this study we observed that exposure of infanticidal virgin males to a pup in wire mesh ball resulted in a significantly increased number of c-Fos- and eYFP-positive $Me^{Cartpt}$ neurons as compared with a wire mesh ball exposure alone (control) (Figure 4A-C).

Next, we aimed to address the causal relationship between synapse plastic changes in the cMPOA and behavioral changes. To address the behavioral causality of the impaired Me-cMPOA inputs, we infused an AAV vector encoding vLWO into the Me of virgin Cartpt-Cre mice and two optic fibers were bilaterally implanted above the cMPOA for optogenetic stimulation. Green light was delivered to the cMPOA during behaviors toward pups being observed (Figure 4D). The latency to first sniffing did not differ significantly between the vLWO group and control group (Figure 4E). However, the proportion of vLWO-expressing mice that did not show infanticidal behavior was significantly larger than in the control group on 4 successive days (Figure 4F and 4G). After the 4-day experiments with green light delivery, we examined the behavioral pattern toward pups

without green light delivery for some individuals. The proportion of vLWO group mice that showed infanticidal behavior did not differ between day 4 (with light) and post-test (without light) (Figure S4). Similar results were observed in the experiments, in which Me input to cMPOA was inhibited in vGAT-IRES-Cre mice (Figure 5). Taken together, these data suggest that $Me^{Cartpt}$ neurons normally serve to suppress cMPOA neurons and promote infanticidal behavior.

**Paternal experience enhances inhibitory transmission in the BSTrh through a postsynaptic mechanism**

We have demonstrated that the decreased inhibition of MPOA by Me input upon experiences with female is a key event for suppressing the infanticide in the FGE. However, about half of FGE mice still show the infanticidal behavior, whereas almost all paternal mice do not show infanticidal behavior[8]. Next, we examined the synaptic change in paternal mice upon experiences with pup.

Downstream structure of the MPOA, the rhomboid nucleus of the bed nucleus of the stria terminalis (BSTrh), has been shown to be activated by infanticidal behavior and negatively regulated by cMPOA[11]. To address the impact of social experiences on the BSTrh synaptic property, we measured the changes in the excitatory−inhibitory (E/I) ratio of the virgin, FGE and paternal groups, in a manner similar to our previous studies[26]. The average amplitude of IPSPs evoked by electrical stimulation of the stria terminalis (Figure 6A) was enhanced in the BSTrh of the paternal group compared to FGE and virgin groups (Figure 6B). However, the average eEPSP amplitudes did

not differ significantly between these groups (Figure 6C). These data suggest that, in the paternal mice, increased inhibition in the BSTrh critically takes place following the disinhibition in the Me–cMPOA pathway as was seen in FGE mice.

We hypothesized that the cMPOA plays a critical role in the increase of inhibition in the BSTrh. To evaluate this hypothesis, we specifically lesioned the MPOA. To this end, we bilaterally injected NMDA into the cMPOA in virgin and paternal mice (Figure 6D and S5) and, 3 to 9 days later, performed whole-cell recordings from BSTrh. In the BSTrh of ipsilaterally lesioned paternal mice, the average eIPSP amplitude was significantly smaller than unlesioned paternal mice (Figure 6E). These data strongly suggest that the increased inhibitory input to the BSTrh is mediated by the cMPOA in mice showing paternal behavior. It should be noted that cMPOA fiber inputs into BSTrh were not likely stimulated to evoke synaptic responses in the current protocol because cMPOA lesion unchanged eIPSP amplitude in virgin mice (Figure 6F).

We next addressed if this increased inhibition onto the BSTrh takes place through a pre- or post-synaptic mechanisms. There were no significant differences in passive membrane properties among the three groups (Table S4). We carried out patch-clamp analysis on BSTrh of paternal group mice and found out that while an inclusion of the GDPβS in the pipette does reduce the amplitude of eIPSPs to the level of virgin group (Figure 6G), eEPSP did not show obvious changes (Figure 6H). These data suggest that the increased eIPSP amplitude in the BSTrh occurs mostly by postsynaptic mechanisms. We also analyzed the paired-pulse ratios to compare the release probability from

presynaptic terminal and found out that the ratio of eEPSCs and eIPSCs did not differ between paternal and virgin groups (Figure 6I). Altogether, we conclude that the cMPOA in the paternal mice mediates plastic changes at GABA synapses in the BSTrh mainly by postsynaptic mechanisms, and these sequential events are centrally involved in the fundamental switch in the paternal behaviors of the father animals.

## Discussion

The results showed that multi-step plastic changes in synapses correlate with the transition from infanticidal to parental behavior in male mice. The inhibitory synapses from $Me^{Cartpt}$ neurons in the cMPOA were impaired by interactions with females. This plastic change in synapses is the potential trigger for the behavioral transition from virgin to FGE. Our targeted cMPOA area are composed by *Galanin*-positive neurons (Fig 1D-G), consistent with the previous reports that the activation of *Galanin*-positive MPOA neuron cause inhibition of aggressive behavior toward pup[12,14]. In addition, the shift from FGE to paternal was accompanied by an increased BSTrh inhibition. These plastic changes caused the change of balance of excitatory–inhibitory synaptic transmission (E/I balance), which correlated positively with the neuronal activity of the cMPOA and BSTrh, when virgin or paternal males contacted with pups.

It was previously reported that the number of males showing infanticide decreased about two weeks after ejaculation without cohabitation with the female partner[7,27]. This discrepancy may

be due to strain differences or by the different experimental/breeding environments. The behavior of males toward pups appears to be controlled by factors triggered by ejaculation, which remain effective for several subsequent weeks, thus preventing infanticide of the male's own offspring. Followingly, additional mechanisms, such as activation of oxytocinergic neuron in paraventricular nucleus of hypothalamus to initiate parental care[28], would complete a series of behavioral changes of male, from aggression to parenting onset.

The Me has been implicated in various social behaviors, including social investigation, mating, and aggression[29-33]. In males, the functional association between the Me and the MPOA is critical for mating behavior[34,35]. The Me comprises several subdivisions with distinct projections and cell types[36,37], including the MePD, which is a sexually dimorphic nucleus crucial for aggressive behaviors[29,31,38,39]. We found the level of pup exposure-induced c-Fos expression in the VNO and MePD was higher in infanticidal virgins than in paternal male mice[8]. On the other hand, the eIPSP amplitude in cMPOA neurons of paternal mice elicited by the stimulation of axonal fibers derived from Me was reversed by intracellular GDP-βS infusion (Figure 1O). These data suggest that both decreased efficacy in synaptic transmission in cMPOA neurons, which we report, and hypoactivity of MePD neurons likely contribute to behavioral selection in male mice. However, the notion that the decrease of Me-to-cMPOA inputs in paternal mice causes a behavioral transition from infanticide to parenting can be overly simplistic, since other brain areas should also provide inputs into the cMPOA and can be modified by mating experiences. Further research is needed to elucidate this

phenomenon of behavioral transition in male mice.

Although we utilized Cartpt-Cre mice to map the Me−cMPOA pathway, Cart may function as a neurotransmitter[40] and so influence Me to MPOA transmission. However, agonists and antagonists specific for Cart transmission have not been identified, so we could not address the influence of Cart released from the Me. In this study, we confirmed that manipulation of Me inputs to the cMPOA in vGAT-IRES-Cre mice led to behavioral changes like those observed in Cartpt-Cre mice (Figure 5). By considering data showing disinhibition in the cMPOA (Figure 1 and 2), we consider that the plastic changes of GABAergic transmission at Me synapses strongly contribute to the shift from infanticide to paternal behavior. On the other hand, we detected EPSCs by optical stimulation of Me inputs into the cMPOA of Cartpt-Cre mice. Therefore, it is possible that subpopulation of Me neurons might specifically control some cMPOA neurons and the associated behavioral pattern. The MPOA contributes to several types of intrinsic behaviors, which in turn activate the MPOA according to different patterns[11,23,32,33,41-44]. However, the mechanisms underlying the expression of one appropriate behavior remains unknown. Suppressing the accessory olfactory signals mediating the Me, presumably changes neural activity patterns in the cMPOA. This is supported by the results that temporal disinhibition of the Me−cMPOA pathway modifies behavioral patterns and increases cMPOA inter-neuronal network activity, as reflected by the increased frequency of postsynaptic currents (Figure 3). In addition to the Me, other inputs into the cMPOA would drive several inter-neuronal network activity patterns to achieve the multi-functional MPOA and behavioral choices.

317 Several studies report that activation of MPOA neurons in virgin males disturbs infanticide,
318 although parental behavior is not initiated[11,12]. Other studies report that activation of MPOA
319 neurons expressing Esr1 or afferents to ventral tegmental area (VTA) promotes parental behavior,
320 as measured by the latency to retrieve pups to the nest[22,23]. Here, the basal motivation for parenting
321 should be carefully distinguished from the behavioral choice toward the pups.

322 Uncovering the primary trigger of cMPOA plastic changes would promote the
323 understanding of how mammalians become parental. Neither mating nor cohabitation with a
324 pregnant female caused sufficient cMPOA disinhibition (Figure S2B and S2C). Because no
325 significant cMPOA disinhibition was observed in virgin males co-housed with a late-gestation
326 pregnant female (the VMLG group), the sensory inputs from pregnant females were unlikely to
327 induce synaptic changes in the cMPOA (Figure S2D and S2E). However, our cohabitation protocol
328 lasted only 3 days; it is possible that longer cohabitation is required for cMPOA disinhibition,
329 although longer cohabitation may be confused by the Bruce effect (i.e., spontaneous pregnancy
330 termination triggered by the scent of an unfamiliar male). Moreover, mating experience without
331 cohabitation with the female partner until late gestation did not change the GABAergic
332 transmission in the cMPOA. We are focusing on the previous reports that mating experiences
333 increase the dopamine turnover[45] and that plastic changes of the expression level of dopamine $D_2$
334 receptor in the MPOA were reported[46]. Because the function of dopamine receptors can change over
335 time[47,48], this may help explain the behavioral transition triggered by the social experience with

female partners. We observed that intracellular GDPβS infusion into cMPOA neurons reversed eIPSP amplitude and the ratio of inhibitory- to excitatory-dominant neurons (Figure 1O, and 2G). These data suggest that postsynaptic $GABA_A$ receptor activity on cMPOA neurons is downregulated (i.e., neuronal disinhibition) by intracellular signals triggered in response to social experience with females. Multiple signaling molecules are reported to be involved in the function of $GABA_A$ receptors[49]. Moreover, altered gene expression levels among virgin, FGE, and paternal mice were recently reported[50]. Among them, the intracellular signaling molecules controlled by GPCR or small G proteins are one of the possible targets to address the mechanisms of plastic changes in the cMPOA.

Interestingly, unlike the synaptic changes in the $Me^{Cartpt}$ - cMPOA pathways of FGE mice, an inhibitory shift was observed in the BSTrh E/I balance, which was induced by the caring experience (Figure 6). What is the biological significance of the increased BSTrh inhibition? Like previous report[11], we observed that BSTrh inactivation by hM4Di significantly delayed infanticidal behavior in virgin male mice without parental behavior initiation (Figure S6). This suggests that BSTrh does not block parental behavior directly. Considering the time course for increased inhibition between FGE and paternal mice, BSTrh plastic changes could contribute to pup sensitization, which underlie the onset of pup caring. The cMPOA lesions reversed the increased BSTrh inhibition in paternal mice to the level of virgin mice, suggesting that the inhibitory transmission of BSTrh was controlled by cMPOA (Figure 6D and 6E). This is supported by the

following facts (1) cMPOA neurons project into the BSTrh and (2) unilateral lesion of the cMPOA increases the number of c-Fos positive neurons in the ipsilateral BSTrh of mice exposed to pups[11]. Because of increased BSTrh inhibition in paternal mice is sensitive to intracellular GDPβS infusion (Figure 6G), some metabotropic receptors of neurotransmitter or peptide may be influencing BSTrh during and/or after pup sensitization. The cMPOA neurons activated during parental behavior contain many kinds of neurotransmitters, including Galanin, neurotensin, and tachykinin2[10,51]. Moreover, the anterior commissural nucleus, adjacent to the cMPOA, contains the third largest population of magnocellular oxytocin neurons. Therefore, cMPOA neurons or adjacent neurons may directly and persistently control $GABA_A$ receptor activity in the BSTrh of paternal mice via metabotropic receptors.

Converging data suggest that the cMPOA neurons contribute to both infanticide inhibition and parental behavior by modifying the inter-neuronal network and projecting to the downstream including BSTrh. There is no doubt that uncovering the relevant MPOA subgroup for each function requires the analysis of neural circuits. Moreover, understanding the modulatory mechanism of synaptic plasticity in the cMPOA and BSTrh may provide evidence for possible interventions in parental stress and subsequent child maltreatment.

**Author contributions**

TA conceived the study with support from KOK. TA, TS and MM designed the experiments. TA, KI,

374 and KS conducted the behavioral experiments. TA and KI performed stereotaxic surgeries. TA, YT,
375 KI, KS, YH, SM and SS performed histological experiments. TA and HU performed whole-cell patch
376 clamp recordings. TM, TS and SH developed the AAV virus expressing vLWO. TA and HO prepared
377 sample for RNA sequence and YS, MS and KS analyzed data. TA wrote the manuscript with support
378 from KOK and YT. All authors contributed to editing the manuscript.
379

380 **Acknowledgements**

381 This work was supported by Japan Society for the Promotion of Science (JSPS) KAKENHI Grant
382 Number 25713044, 16K19747, 16H06279 (PAGS), 18K07584, 21K07494 (to TA), 26282220 (to KOK),
383 15K01832 (to TM), 19H03328, 20H05068 (to HO), Suzuken Memorial Foundation (to TA), Narishige
384 Neuroscience Research Foundation (to TA), Nishinomiya Basic Research Fund, Japan (to TA), and
385 the fellowship of Special Postdoctoral Researchers Program at RIKEN (to TA), Hokkaido University,
386 Global Facility Center (GFC), Pharma Science Open Unit (PSOU), funded by MEXT under "Support
387 Program for Implementation of New Equipment Sharing System," RIKEN Brain Science Institute
388 (2011-2015 to KOK), Deutsche Forschungsgemeinschaft He2471/18 Priority Program (SPP1926),
389 SFB874, SFB1280, DFG2471/21, DFG2471/23 project B10 (to SH). We appreciate Dr. Goichi Miyoshi
390 for critically reading this manuscript prior to submission, Dr. Shigeyoshi Fujisawa and Kazunari
391 Miyamichi for supporting genetically modified mice transportation, RIKEN Research Resource
392 Center for maintenance of animals, Kiyomi Imamura, Terumi Horiuchi, Dr. R. Jude Samulski and

393 the UNC Vector Core for helpful supports.

394

## STAR Methods

### Animals

The Animal Experiment Committee of the RIKEN Brain Science Institute and Institutional Animal Care and Use Committee at Hokkaido University approved all animal experiments, which were conducted in compliance with the National Institute of Health guidelines for the care and use of laboratory animals.

### Animal maintenance and male exposure to different levels of mating and paternal experience

Most C57BL/6J male mice were bred at the RIKEN Brain Science Institute and Graduate School of Pharmaceutical Sciences, Hokkaido University unless specially described. For the BDA (Thermo Fisher Scientific) tracer injection into Me (Figure 1A-C and S1), we utilized C57BL/6J male mice from Japan SLC. Cartpt-Cre mice (Jackson Laboratory, stock number 009615), vGAT-IRES-Cre mice (Jackson Laboratory, stock number 016962) and Ai9 (Jackson Laboratory, stock number 007909) were bred at the Graduate School of Pharmaceutical Sciences, Hokkaido University. We backcrossed vGAT-IRES-Cre mice with C57BL/6J mice at least five generations after arrival from Jackson Laboratory. Mice were housed in individually ventilated cages and provided ad libitum access to water and food and maintained under a 12-h light/dark cycle in cages lined with TEK Fresh Standard bedding (Envigo). Mice were weaned at postnatal day 28 (P28). All mutant heterogenic mice were co-housed with wild-type mice until the experiments. To produce paternal group mice, a virgin male mouse was housed with a female for mating. After delivery, the male

stayed with pups for 3 days. All paternal group males experienced one delivery and were used for experiments within 20 days after the birth of pups. If pups did not survive for more than 3 days, the male was not included in the paternal group for experiments. Other virgin male mice were mated and co-housed with a female only until late gestation but not delivery, termed 'fathers in gestation experience' (FGE) mice.

Stereotaxic surgery

BDA (1.25 μg/ dissolved in 12.5 nL 0.1 M phosphate buffer), N-methyl-D-aspartic acid (NMDA, Sigma-Aldrich, 20 mg/ml in saline), and AAV5-EF1α-DIO-hChR2(H134R)-eYFP ($6.6 \times 10^{12}$ genome copies/ml, provided by Vector Core at the University of North Carolina (UNC) at Chapel Hill, UNC vector core), AAV5-EF1α-DIO-eYFP ($5.6 \times 10^{12}$ genome copies/ml, UNC vector core), AAV10-EF1α-DIO-vLWO-eGFP-5HT1A ($3.7\times 10^{13}$ or $1.8 \times 10^{13}$ genome copies/ml, UNC vector core), AAV10-EF1α-DIO-eYFP ($1.2 \times 10^{14}$ or $3.7 \times 10^{13}$ genome copies/ml, UNC vector core), rAAV2-EF1a-DO_DIO-tdTomato_EGFP-WPRE (more than $7.0 \times 10^{12}$ vg/ml, Addgene), AAV2-hSyn-HA-IRES-eGFP ($3.3 \times 10^{12}$ genome copies/ml, UNC vector core), and AAV2-hSyn-HA-hM4Di(Gi)-IRES-mCitrine ($5.6 \times 10^{12}$ genome copies/ml, UNC vector core) (100–400 nL/hemisphere), were administered under anesthesia. Briefly, 2–3-month-old male mice were anesthetized by intraperitoneal (i.p.) sodium pentobarbital (30 mg/kg) or the mixture of medetomidine hydrochloride (0.3mg/kg), midazolam (4mg/kg), butorphanol tartrate (5 mg/kg)[52], and local subcutaneous (s.c.) lidocaine hydrochloride. The skull

433 was exposed and holes drilled for stereotaxic injection. Glass capillaries of ~50 μm tip diameter were
434 filled with oil and backfilled with the test drug or AAV vector. Injection was targeted by referring to
435 the Mouse Brain Atlas of Flanklin & Paxinos (2007) coordinates for the Me (AP −1.5 mm, ML 2.1
436 mm, DV −5.4 mm and AP −1.2 mm, ML 1.9 mm, DV −5.6 mm), cMPOA (AP 0.1 mm, ML 0.55 mm,
437 DV −5.1 mm), and BSTrh (AP −0.1 mm, ML 1.2 mm, DV −4.2 mm). After injection, the skin was
438 closed with a nylon suture. Mice were kept in single housing 3–4 days for recovery. Mice injected
439 with AAV vectors were then maintained under group housing for more than 4 weeks to allow for
440 expression of vector genes. One week before behavioral testing, optic fibers were implanted into the
441 targeted area as described below.
442
443 Histological analysis
444 Mice were anesthetized by sodium pentobarbital (50 mg/kg, i.p.) and transcardially perfused with
445 4% paraformaldehyde (PFA) dissolved in phosphate buffered saline (PBS, pH 7.4). Brains were
446 removed from the skull and post-fixed overnight in PFA at 4 °C, followed by incubation in PBS/20%
447 sucrose for 1 day and PBS/30% sucrose for 1–2 days. Brains were then embedded in O.C.T.
448 Compound (Sakura Finetek) at −80 °C and sectioned at 40 μm using a Cryostat (Leica Biosystems)
449 unless otherwise indicated. Some brains were used to prepare sections for electrophysiological
450 analysis. In the case of BSTrh recording after MPOA lesion, serial slices including MPOA were
451 sectioned at 80 μm in cutting solution (see below) using a Leica VT1200 Semiautomatic Vibrating

Blade Microtome (Leica). These slices and the slices including BSTrh used for electrophysiological analysis were fixed in 4% PFA and immunostained.

For fluorescent immunohistochemical staining, brain slices were incubated in PBS containing 0.1% Triton X-100 (PBST) for more than 15 min and then in 0.4% Block Ace (Dainihon-Seiyaku) for an hour. Slices were then incubated at 4 °C overnight in Block Ace solution containing primary antibody. After several rinses in PBST, slices were incubated in PBST containing secondary antibody at room temperature. Table S5 shows antibody list.

To stain the BDA anterograde tracer, sections were incubated with Alexa 568-conjugated streptavidin (1:500, Thermo Fisher Scientific) for 2 hours. After washout of the secondary antibody or streptavidin, slices were mounted on glass slides with VECTASHIELD Mounting Medium (Vector Laboratories). For 3, 3-diaminobenzidine (DAB) staining, immunolabeled slices were incubated in 0.1 M glycine for 10 min, 0.5% $H_2O_2$ for 30 min, and VECTASTAIN ABC reagent (Vector Laboratories) overnight at 4 °C. After rinsing several times with PBST, the slices were incubated with Vector DAB Substrate (Vector Laboratories) including nickel chloride for about 5 min. The stained slices were mounted on gelatin-coated glass slides and dried. After nissl staining, slides were treated with Softmount (Wako). Labeling of *Galanin* positive neurons followed modified protocol of *in situ* hybridization chain reaction (HCR) using short hairpin DNAs[53,54] using probes listed in Table S6. Fixed brain section re-sliced at 75 µm after patch clamp recording with internal solution containing 1% biocytin (Sigma) and 100 nU RNase inhibitor (Promega), or 30 µm brain

471 section fixed by 4% PFA were soaked in methanol for 10 minutes. After washing with PBST, the
472 sections were prehybridized for 10 min at 37°C in a hybridization buffer containing 10% dextran
473 sulfate, 1× standard saline citrate (SSC), 0.1% Tween 20, 50 µg/ml heparin, 1× Denhardt's solution.
474 The sections were moved to another hybridization solution containing a mixture of 20 nM split-
475 initiator probes, and incubated overnight at 37°C. For *in situ* HCR, 3 µM hairpin DNA solutions
476 were separately snap-cooled before use. The sections were incubated in amplification buffer (10%
477 dextran sulfate in 5× SSCT) with 60 nM hairpin DNA pairs for 2 hours at 25°C. Then, the samples
478 were washed with PBST three times at room temperature.

479 Immunofluorescence images were captured using an incident-light fluorescence microscope
480 (Leica DM6000B, Leica), confocal laser-scanning microscope (FV-10, Olympus), or fluorescence
481 microscope (BZ-X700, Keyence). To allow for comparison among trials, the contrast and brightness
482 of all photographs were adjusted linearly and uniformly using Adobe Photoshop CS5 (Adobe
483 Systems) unless specially described. For the lesion study, sections were immunostained with anti-
484 NeuN antibody to confirm cell death in the target area. The loss of NeuN-immunoreactive cells in
485 the NMDA-injected group was compared with the saline group to judge the lesioned area.

486

487 Electrophysiology

488 Electrophysiological recordings were performed as described previously[26]. The artificial cerebral
489 spinal fluid (ACSF) contained 126 mM NaCl, 2.5 mM KCl, 1.25 mM $NaH_2PO_4$, 1 mM $MgCl_2$, 2 mM

$CaCl_2$, 26 mM $NaHCO_3$, and 10 mM glucose (pH 7.3). For a cutting solution, NaCl in ACSF was replaced with the same concentration of choline chloride. Mice were injected with pentobarbital (30 mg/kg, i.p.) followed by transcardiac perfusion of ice-cold cutting solution. The brains were removed, and 230-μm brain slices including the target area prepared in ice-cold choline chloride-based cutting solution using a Leica VT1200 Semiautomatic Vibrating Blade Microtome. Brain slices were stored in warmed ACSF at 32 °C for 20–30 min and then kept at room temperature until recording.

For electrophysiological recordings, slices were superfused with 32 °C–34 °C ACSF at 2–4 mL/min in a chamber mounted on a microscope. Neurons were identified using a 40× or 60× lens and an infrared camera (IR-1000, DEGE-MTI). Glass electrodes (World Precision Instruments) of 4–9 MΩ resistance were used for whole-cell patch clamp recordings in response to electrical stimulation using ~0.5 MΩ glass electrodes containing ACSF. Recording electrodes were filled with a potassium-based internal solution (132 mM K-gluconate, 3 mM KCl, 10 mM HEPES, 0.5 mM EGTA, 1 mM $MgCl_2$, 12 mM Na-phosphocreatine, 4 mM Mg-ATP, 0.5 mM Na-GTP, 0.2-0.3 % biocytin, pH 7.25) and signals were recorded using an Axopatch 700B amplifier (Molecular Devices). Only cells with access resistance <30 MΩ and exhibiting action potentials with >60 mV amplitude evoked by positive current injection were included in the analysis. Whole-cell currents were filtered at 3 kHz. The liquid junction potential (11 mV) was compensated. Stimulating electrodes were placed at the dorsal BSTrh or cMPOA to stimulate stria terminalis. To activate the ChR2-expressing axon terminals, we utilized a LED (465 nm, LEX2-LZ4-B, Brainvision Inc.). To activate the vLWO-

509 expressing neurons, green light generated by a 100 W mercury lamp (U-RFL-T) was applied
510 through a fluorescence band pass filter (520-550 nm) (Olympus). Red light was provided by Fiber-
511 Coupled LED (625 nm, Thorlabs). Evoked synaptic currents and potentials were measured at least
512 three times at the same stimulus intensity and averaged. Responses with action potentials were
513 omitted from the analysis. We recorded evoked excitatory postsynaptic potentials (eEPSPs) and
514 eEPSCs at a holding potential of −85 mV in the presence of 100 μM picrotoxin. eIPSPs were
515 recorded at −65 mV and eIPSCs at −60 mV in the presence of 20 μM CNQX and 20 μM MK-801. In
516 experiments using optogenetic suppression using vLWO, slices were also perfused with 25 μM 9-cis-
517 retinal, 0.1% dimethyl sulfoxide, 0.025% (±)- α-tocopherol and 0.2% bovine serum albumin.
518
519 Behavioral test
520 The tests of paternal behavior toward pups were performed as described previously[26]. Mice were
521 housed individually in cages containing new purified paper bedding (Alpha-Dri, Shepherd Specialty
522 Papers) and a cotton square (Nestlet, Ancare). After 1–2 days, three pups aged 1–6 days were placed
523 into the cage corner avoiding the nest. Tests were performed once each day for 30 min on 4
524 successive days during the daytime unless otherwise indicated. The endpoint of the aggressive
525 behavior toward pups to terminate the experiments was 2-s screams or visible wounds on the pup
526 skin. Wounded pups were immediately euthanized. The paternal behavioral score was evaluated
527 according to previous reports as follows: 4 = all pups were retrieved, 3 = 1 or 2 pups were retrieved,

2 = no pup was retrieved, 1 = at least one pup was attacked >3 min after placement in the test cage, and 0 = at least one pup was attacked within 3 min after placement in the test cage.

For c-Fos mapping, the procedure was modified from a previous study[8]. Briefly, mice were exposed to a pup protected inside wire-mesh ball (tea balls, 45 mm diameter; Minex Metal, Tsubame, Japan) with about 10 holes (5 mm diameter) placed in a cage corner avoiding the nest for 30 min. Ninety minutes later, the adult male was anesthetized with pentobarbital (50 mg/kg, i.p.) and transcardially perfused with 4% PFA/PBS for brain isolation as described above. The c-Fos immunoreactive cells were counted automatically by Image J software (National Institutes of Health, Bethesda, MD, USA).

Optogenetic and chemogenetic manipulation of neural activity in vivo

Zirconia ferrules optical fibers (Thorlabs) of 200 μm diameter core (NA = 0.37) were cut and polished for >70% coefficient of transmission. These constructs were bilaterally implanted into the mouse brain area 1-mm above the target area and fixed with dental cement. After the mouse had recovered from the surgery (one week later), the optic fibers were connected via Ceramic Split Mating with 1×2 Branching Fiber-optic Patch Cords-Glass (0.37 NA, Doric Lenses) to a diode laser (450 nm or 532 nm, Changchun New Industries Optoelectronics Tec.) through a FC/PC connector. Averaged light power at the tips between the bilateral fiber tips was set to 30−40 mW (450 nm) or 10−12 mW (532 nm). Light pulses were controlled by TTL Pulse Generators (Doric Lenses). After connecting

the fibers, experimental mice were allowed free actiTon for 15 min. During the last minute of the behavioral test, mice received constant light on for 20 s without light pulses followed by a 10-s off period. This photostimulation protocol was continued throughout the 30-min behavioral experiment. After the behavioral experiments, animals were perfused with 4% PFA to prepare the brain slices. Only animals with bilateral expression of fluorescence labeled fiber and the bilateral optic fibers above targeted area between 0.3-1.0 mm from the targeted area were included for the data analysis. For the chemogentic silencing, we infused CNO (2.0 mg / kg, i.p.) and observed the behavioral pattern 30-35 min later. After the behavioral experiments, we immunostained the brain slices with anti-GFP. Only animals with bilateral expression of fluorescent signal in the targeted area were included for the data analysis.

RNA-seq analysis

Mouse brain slices were prepared using essentially the same procedures for electrophysiological experiments. Six cMPOA neurons were manually collected by using 1 ~ 2 MΩ glass electrodes containing ACSF and suspended in cell lysis buffer (0.5% Triton-X100, 0.5 U/μL RNase inhibitor, 5 ng/μL yeast rRNA). The cell samples were immediately frozen and stored at −80°C until starting reverse transcription. Reverse transcription and cDNA library preparation were performed using the Smart-seq2 method[55] with some modifications. Briefly, 12 μM $dT_{30}VN$ primer (5'-AAGCAGTGGTATCAACGCAGAGTAC$T_{30}$VN-3) were added into microtubes containing cell lysates

(final concentration, 1 μM); then, samples were heat-denatured at 70 °C for 3 min, followed by immediate incubation on ice. Next, samples were mixed with a reverse transcription reaction solution containing locked nucleic acid (LNA)-template switching oligo primer (5'-AAGCAGTGGTATCAACGCAGAGTACrGrG+G-3', rG; riboguanosines, +G; LNA-modified guanosine, final concentration of 0.6 μM) and reverse transcriptase (SMARTscribe, Clontech, final concentration of 5 U/μL), and incubated at 42°C for 120 min followed by at 70°C for 10 min to terminate the reaction. The resultant cDNA samples were purified using solid phase reversible immobilization (SPRI) beads (AMPure XP, Beckman Coulter). The purified cDNA samples were amplified by PCR using the IS primer (5'-$NH_2$-AAGCAGTGGTATCAACGCAGAGT-3', final concentration of 0.24 μM) and Tks Gflex DNA polymerase (Takara Bio, final concentration of 0.025 U/μL). The amplified cDNA samples were purified by SPRI beads. The quality and quantity of cDNA sample was confirmed by an Agilent 2100 Bioanalyzer using the High sensitivity DNA kit (Agilent Technology, CA, USA).

The cDNA samples were then processed to generate indexed libraries for sequencing using a NEBNext Ultra II DNA Library Prep Kit for Illumina (#E7645, New England Biolabs Inc., Ipswich, MA, USA), according to manufacturer's instructions. Then, libraries were sequenced for 50-bp single-end reads using HiSeq 3000 (Illumina, San Diego, CA, USA). Output fastq files were aligned to the mouse genome (GRCm38/mm10) using STAR aligner[56]. Library size normalization was performed using R (v.4.1.0) by calculating transcripts per million (TPM). Genes with <5 TPM in all

585 samples were excluded from the analysis. We selected 22 genes for neuronal cluster-mediated social
586 behavior in the MPOA based on previous reports[21]. However, *Oprd1* was excluded because of its low
587 expression. Heatmaps were drawn using gplots (v.3.1.1). Differentially expressed genes (DEGs)
588 between virgin, FGE, and paternal mice were analyzed using DESeq2 (v.1.32.0). Genes with a false
589 discovery rate-adjusted $p \leq 0.05$ and a $\log_2$ fold change $\geq 2$ in either direction were considered DEGs.
590
591 **Statistical analysis**
592 Group means were compared by Fisher's exact test, the two-tailed t-test, one-way or two-way
593 repeated measures ANOVA followed by a post hoc test as indicated. All statistical tests were two-
594 tailed and conducted with GraphPad Prism software 6 and 9 (GraphPad Software, Inc., La Jolla, CA,
595 USA). A P-value < 0.05 was deemed statistically significant. Statical data was written in the figure
596 legends and Table S7.
597
598 **Data availability**
599 All data that support the findings presented in this study are available from the corresponding
600 author upon request. The raw sequences have been deposited in the DNA Data Bank of Japan
601 (DDBJ) under the DDBJ BioProject umbrella with accession number PRJDB8470, and to the DDBJ
602 Read Archive DRA008585 (BioSample ID: SAMD00175991- SAMD00176002).
603

604 **Lead contact**

605 Further information and requests for resources and reagents should be directed to and will be

606 fulfilled by the lead contact, Taiju Amano (tamano@pharm.hokudai.ac.jp).

607

608 **Figure Legends**

609 Figure 1 The medial amygdala sends projections to the cMPOA

610 (A) Medial amygdala in the parasagittal section. HC; hippocampus, cp; cerebral peduncle, opt; optic

611 tract, EA; extended amygdala, AHi; amygdalohippocampal area, MeP; medial amygdaloid nucleus,

612 posterior part, MeA; medial amygdaloid nucleus, anterior part, LOT; nucleus of the lateral olfactory

613 tract, AA; anterior amygdaloid area.

614 (B) Representative images of the Me stained with anti-Cart visualized with Alexa 488 and BDA

615 visualized with Alexa 568-conjugated streptavidin (magenta). Scale bar = 200 μm.

616 (C) Representative images of the Me injected with the tracer BDA in the MPOA. Parasagittal

617 sections are shown from lateral to medial. Fixed sections were visualized with Alexa 568-conjugated

618 streptavidin (magenta). In parallel, fixed sectioned were immunostained with anti-NPI and

619 visualized with Alexa 488 (green). Main targeted area as the cMPOA (right, lateral 0.5 mm) was

620 represented as the area of yellow line by reference to our previous study[11]. Scale bar = 200 μm.

621 (D) left, summary of experimental procedure. middle, RNA-seq identification of candidate gene

622 expressed in the cMPOA neurons. Heatmap showing a *z*-scored TPM of selected genes for neuronal

cluster-mediated social behavior in the MPOA[21]. n = 4 (virgin), 4 (FGE), and 4 (paternal). right, Social experiences of virgin, FGE, and paternal group mice.

(E) Representative images of the MPOA. *Galanin* mRNA Alexa 647 -conjugated hairpin DNA (#S23) (magenta), streptavidin conjugated with FITC (green) and DAPI (blue). (e1-e3) magnified images corresponding area in (e), Scale bar = 200 μm for (e, left) and 20 μm for (e1-e3)

(F) Representative images of cMPOA neurons after whole-cell patch-clamp recording. Biocytin was infused from recording pipette. Fixed sections visualized with Alexa 488-conjugated streptavidin (green) and *in situ* HCR for *Galanin* mRNA Alexa 647 -conjugated hairpin DNA (#S23) (magenta). Scale bar = 20 μm.

(G) Ratio of *Galanin* positive cMPOA neurons targeted for whole-cell patch-clamp recording.

(H) Fixed sections were immunostained with anti-NPI visualized with a secondary antibody conjugated to Alexa 488 (green) and immunostained with anti-ERα visualized with a secondary antibody conjugated to Alexa 568 (magenta). Scale bar = 300 μm.

(I) Fixed sections were visualized with *in situ* HCR for *Galanin* mRNA Alexa 647 -conjugated hairpin DNA (#S23) (magenta), immunostained with anti-ERα visualized with a secondary antibody conjugated to Alexa 488 (green), and DAPI (blue). Scale bar = 200 μm. f, fornix, ac, anterior commissure.

(J) Representative images of cMPOA neurons after whole-cell patch-clamp recording. Biocytin was infused from recording pipette. Fixed sections visualized with Alexa 568-conjugated streptavidin

642 (magenta) and immunostained with anti-ERα and secondary antibody conjugated to Alexa 488
643 (green). Scale bar = 20 μm.
644 (K) Ratio of ERα positive cMPOA neurons targeted for whole-cell patch-clamp recording.
645 (L) Schematic image of the recording and stimulating electrodes on a parasagittal section including
646 the cMPOA. BSTv; bed nucleus of the stria terminalis, ventral part,
647 (M) Input–output curves of stimulus-evoked IPSPs from the *Galanin* positive cMPOA of virgin mice
648 (n = 12 cells; 7 animals) and FGE mice (n = 7 cells; 5 animals). Values are presented as the mean ±
649 standard error. (bottom) Representative traces used to construct input–output curves (40, 80, 120,
650 160, and 200 μA stimuli). Two-way RM ANOVA, $F(1, 17) = 4.964$, $P = 0.0397$ followed by Holm-
651 Sidak post hoc test, *$P < 0.05$, **$P < 0.01$ vs. virgin group.
652 (N) Input–output curves of stimulus-evoked IPSPs from the cMPOA of virgin mice (n = 11 cells; 4
653 animals) and paternal mice (n = 11 cells; 4 animals). Values are presented as the mean ± standard
654 error. (bottom) Representative traces used to construct input–output curves (25, 75, 125, 175 and
655 225 μA stimuli, performed in a different setup and at different stimulation intensity ranges from
656 Figure 1E, 1G and 1H). Two-way RM ANOVA, $F(1, 20) = 10.72$, $P = 0.0038$ followed by Holm-Sidak
657 post hoc test, ***$P < 0.001$, ****$P < 0.0001$ vs. virgin group.
658 (O) Input–output curves of stimulus-evoked IPSPs from paternal mice recorded without (n = 7 cells;
659 2 animals) or with GDPβS (1 mM) in the pipette solution (n = 16 cells; 4 animals). Values are
660 presented as the mean ± standard error. (bottom) Representative traces used to construct

input–output curves (40, 80, 120, 160, and 200 μA stimuli). Two-way RM ANOVA, $F(1, 21) = 6.212$, $P = 0.0211$ followed by Holm-Sidak post hoc test, *$P < 0.05$, **$P < 0.01$ vs. paternal group without GDPβS.

(P) Input–output curves of stimulus-evoked EPSPs from the cMPOA of virgin mice (n = 21 cells; 3 animals) and paternal mice (n = 14 cells; 3 animals). Values are presented as mean ± standard error. (bottom) Representative traces used to construct input–output curves (40, 80, 120, 160, and 200 μA stimuli). Two-way RM ANOVA, $F(1, 33) = 0.7974$, $P > 0.05$.

Figure 2 Cre-positive neuron in the medial amygdala of Cartpt-Cre mice project to cMPOA neuron

(A) Representative images of the MePD in Cartpt-Cre × Ai9 reporter mice. Among MePD neurons immunostained with anti-NeuN antibody visualized with a secondary antibody conjugated to Alexa 647 (blue), 21.2% Cartpt neurons (magenta) were tdTomato positive (1 male, 1 female). Scale bar = 300 μm. opt; optic tract, LV; lateral ventricle, AHi; amygdalohippocampal area, MePD; posterior-dorsal medial amygdala, MePV; posterior-ventral medial amygdala

(B) AAV5-EF1α-DIO-eYFP or AAV5-EF1α-DIO-ChR2-eYFP was injected into the Me of Cartpt-Cre mice. After the expression of eYFP with/without ChR2, whole-cell patch clamp recordings were performed from cMPOA neuron in parasagittal sections of virgin and FGE mouse brain.

(C, D) Representative images of eYFP emission from Me (C) and MPOA (D). $Me^{Cartpt}$ neurons sent projection fibers into the MPOA. Scale bar = 200 μm.

(E) (left)Schematic image of the recording electrodes on a parasagittal section including the cMPOA. Input fiber from $Me^{Cartpt}$ expressed ChR2 were stimulated by blue light application. BSTv; bed nucleus of the stria terminalis, ventral part, (right) Diagram of dominant responses of IPSC and EPSC with opposite current direction as that of GABAergic and glutamatergic ionotropic receptors.

(F) Representative traces of blue light-evoked IPSCs and EPSCs in IPSC- and EPSC-dominant cMPOA neurons. When $Me^{Cartpt}$ neurons were injected with control AAV virus, no responses to optical activation were observed in cMPOA neurons.

(G) Relative frequencies of excitatory- and inhibitory-dominant cMPOA neurons in virgin mice (n = 12 cells; 4 animals), FGE mice (n = 14 cells; 3 animals), and FGE mice with GDPβS (1 mM) in the pipette solution (n = 9 cells; 2 animals). A significant difference in the ratio of excitatory- to inhibitory-dominant cMPOA neurons between virgin and FGE group mice was observed (Fisher's exact probability test, **P = 0.0048). A significant difference in the ratio of excitatory- and inhibitory-dominant cMPOA neurons between FGE mice and FGE mice with GDPβS (1 mM) in the pipette solution (FGE + GDPβS group) was also observed (Fisher's exact probability test, #P = 0.0131).

Figure 3 The modulation of Me inputs into the cMPOA

(A) AAV10-EF1α-DIO-vLWO-eGFP or AAV10-EF1α-DIO-eYFP were injected into the Me of Cartpt-Cre mice and whole-cell recordings were obtained from fluorescent-labeled Me neurons.

(B) Representative resting membrane potential traces recorded from a $Me^{Cartpt}$ neuron expressing vLWO. Green light was applied for 20 s (green bar).

(C) Effects of green light application on the resting membrane potential in the $Me^{Cartpt}$ neurons expressing vLWO. The data are shown as the averaged potentials between −6 s and −1 s before the onset of green light application (pre-green light) and between 5 s and 10 s after the onset of green light application (green light). Lines represent the data obtained from individual neurons (n = 5), and bars represent the averaged data obtained from five neurons. **P = 0.0017, two-tailed paired t-test (t = 7.466, df = 4), compared with pre-green light application.

(D) Representative resting membrane potential traces recorded from a $Me^{Cartpt}$ neuron expressing control eYFP. Green light was applied for 20 s (green bar). Five animals were excluded due to exclusion criteria.

(E) Effects of green light application on the resting membrane potential in the $Me^{Cartpt}$ neurons expressing control eYFP. Lines represent the data obtained from individual neurons (n = 10), and bars represent the averaged data obtained from nine neurons. P = 0.6308, two-tailed paired t-test (t=0.4975 df=9), compared with pre-green light application.

(F) AAV5-DIO-ChR2(H134R)-mCherry and AAV10-EF1α-DIO-vLWO-eGFP-5HT1A was injected into the Me of Cartpt-Cre mice and whole-cell recordings were obtained from cMPOA neurons.

(G) Representative images of the Me expressing eGFP and mCherry. Scale bar = 200 μm.

(H) Representative traces of blue light-evoked IPSCs in the cMPOA neurons. Red bar indicates red

light application (2 s).

(I) Effects of red-light application on the blue light-evoked postsynaptic currents in the cMPOA neurons. Lines represent the data obtained from individual neurons (n = 4), and bars represent the averaged data obtained. ***P = 0.0007, two-tailed paired t-test (t=14.25 df=3), compared with pre-red light application.

(J) AAV10-EF1α-DIO-vLWO-eGFP was injected into the Me of Cartpt-Cre mice and whole-cell recordings were obtained from cMPOA neurons.

(K) Representative trace of green light-induced modulation of sIPSCs in the cMPOA neurons. Data were obtained in the presence of CNQX (20 μM) and MK-801 (20 μM). Green light was applied for 20 s.

(L) Effects of green light application on the frequency of sIPSC in the cMPOA neurons. Lines represent the data obtained from individual neurons (n = 25), and bars represent the averaged data. Repeated measures ANOVA, F (1.468, 35.23) = 3.962, P = 0.0396, followed by Dunnett's multiple comparisons post hoc test *P = 0.0332 compared with pre-green light application. One data showed large sIPSC frequency. It was judged as an outlier in Grubbs' test. Without this data point, the same repeated measure ANOVA analysis resulted in F (1.733, 39.87) = 4.149, P=0.0279, indicating that the conclusion remains when leaving out this outlier.

(M) Representative trace of sIPSCs in the cMPOA neurons in the presence of TTX (1 μM).

(N) Application of TTX blocked the green light induced changes of IPSCs frequency. Lines represent

737 the data obtained from individual neurons (n = 12), and bars represent the averaged data. Repeated

738 measures ANOVA, $F(1.236, 13.60) = 0.2769$, $P = 0.6561$.

739

740 Figure 4 Optogenetic manipulation of the $Me^{Cartpt}$–cMPOA input suppressed infanticidal behavior of

741 virgin male mice

742 (A, B) Representative images of c-Fos induction in the Me following pup exposure (A) and in the

743 control Me (B). Fixed sections were stained with anti-c-Fos and visualized with Alexa 647 (magenta).

744 eYFP was expressed by injection of AAV10-EF1α-DIO-eYFP. Scale bar = 200 μm for 10× images.

745 Scale bar = 50 μm for 60× images.

746 (C) Percentage of c-Fos-positive $Me^{Cartpt}$ neurons out of all eYFP-positive $Me^{Cartpt}$ neurons following

747 pup exposure. A pup kept in a metal net to avoid biting attacks was placed in the test cage for 30

748 min (n = 3). An empty metal net was added as a control (n = 3). ****$P < 0.0001$, two-tailed unpaired

749 t-test ($t = 23.41$, $df = 4$).

750 (D) AAV10-EF1α-DIO-vLWO-eGFP-5HT1A or AAV10-EF1α-DIO-eYFP was injected into the Me of

751 Cartpt-Cre mice. Five weeks later, glass fibers were implanted above the cMPOA for pathway

752 stimulation. During the behavioral test, 532 nm green light was applied following a repeated

753 protocol of 20 s on and 10 s off.

754 (E) Latencies to first sniffing were compared between vLWO and control group mice. Two-way RM

755 ANOVA, $F(1, 16) = 1.642$, $P = 0.2183$.

(F, G) Relative frequencies of paternal/infanticidal behaviors toward pups during manipulation of the $Me^{Cartpt}$-to-cMPOA input by vLWO activation. Significant difference in the ratio showing infanticidal behavior between mice expressing vLWO-eGFP (n = 8, F) or eYFP only (n = 10, G) *P = 0.0229, **P = 0.0065, Fisher's exact probability test. Eight animals of vLWO group were excluded due to exclusion criteria.

Figure 5

Optogenetic inhibition of the Me–cMPOA input in vGAT-IRES-Cre mice suppressed infanticidal behavior of virgin male mice

(A) AAV10- EF1α-DIO-vLWO-eGFP-5HT1A or AAV10-EF1α-DIO-eYFP was injected into the Me of vGAT-IRES-Cre mice. Five weeks later, glass fibers were implanted above the cMPOA. During the behavioral test, 532 nm green light was repeatedly applied at 20 s on and 10 s off.

(B) Representative images of eYFP emission from the MPOA of vGAT-IRES-Cre mice (green). Sections including the Me were immunostained with anti-NPI and visualized with a secondary antibody conjugated to Alexa 594 (magenta).

(C) Representative images of eYFP expressed in the Me of vGAT-IRES-Cre mice (green). Sections were immunostained with anti-Cart and visualized with a secondary antibody conjugated to Alexa 594 (magenta). All scale bar = 200 μm.

(D, E) Relative frequencies of paternal/infanticidal behaviors during vLWO activation at the $Me^{vGAT}$

775 input into cMPOA. Significant difference in the ratio of mice showing infanticide between vLWO (n
776 = 7, D) and control (n = 10, E) groups (Fisher's exact probability test, *P = 0.0345).
777
778 Figure 6 Inhibitory synaptic inputs into the BSTrh were potentiated in paternal group mice
779 (A) Whole-cell patch clamp recordings were performed on BSTrh neurons (Rec). To observe the
780 evoked synaptic responses, electrical stimulation was delivered through a stimulating electrode
781 (Stim). rh, rhomboid nucleus; pr, principal nucleus; LV, lateral ventricle; ic, internal capsule; f,
782 fornix; D3V, dorsal third ventricle; GP, globus pallidus; ac, anterior commissure; ST, stria terminalis
783 (B) Input–output curves of stimulus-evoked IPSPs from virgin mice (n = 16 cells; 10 animals),
784 paternal mice (n = 17 cells; 11 animals), and FGE mice (n = 10 cells; 5 animals). Values are
785 presented as the mean ± standard error. (inset) Representative traces used to construct
786 input–output curves (50, 100, 150, and 200 μA stimuli). Two-way RM ANOVA, $F(2, 40) = 5.416$, $P = 0.0083$, followed by Holm-Sidak post hoc test, *$P < 0.05$, **$P < 0.01$ vs. virgin group.
788 (C) Input–output curves of stimulus-evoked EPSPs from virgin mice (n = 9 cells; 6 animals),
789 paternal mice (n = 15 cells; 6 animals), and FGE mice (n = 6 cells; 3 animals). Values are presented
790 as the mean ± standard error. (inset) Representative traces used to construct input–output curves
791 (25 and 100 μA stimuli). Two-way RM ANOVA, $F(2, 27) = 0.4838$, $P > 0.05$.
792 (D) Photographs of the MPOA from sham-operated and NMDA-lesioned mice. Sections were
793 immunostained with anti-NeuN and visualized with DAB. Arrowhead indicates the ventral edge of

794 lesioned area. Scale bar = 500 μm.

795 (E) Input–output curves of stimulus-evoked IPSPs from paternal sham-operated mice (sham; n = 26
796 from 7 mice, NMDA; n = 15 from 6 mice). Values are presented as the mean ± standard error. (inset)
797 Representative traces used to construct input–output curves (25, 75, 125, and 175 μA stimuli). Two-
798 way RM ANOVA, $F(1, 29) = 10.30$, $P = 0.0032$ followed by Holm-Sidak post hoc test, *$P < 0.05$, **$P <$
799 0.01, ***$P < 0.001$ vs. virgin group.

800 (F) Input–output curves of stimulus-evoked IPSPs from sham-operated virgin mice (sham; n = 7
801 cells; 4 animals) and cMPOA-lesioned virgin mice (NMDA; n = 9 cells; 4 animals). Values are
802 presented as the mean ± standard error. (inset) Representative traces used to construct
803 input–output curves (25, 75, 125, and 175 μA stimuli). Two-way RM ANOVA, $F(1, 14) = 0.9177$, $P >$
804 0.05.

805 (G) Input–output curves of stimulus-evoked IPSPs from virgin mice (n = 10 cells; 4 animals) and
806 paternal mice (n = 9 cells; 4 animals) recorded with GDPβS (1 mM) in the pipette solution. Values
807 are presented as mean ± standard error. (inset) Representative traces used to construct
808 input–output curves (50, 100, 150, and 200 μA stimuli). Two-way RM ANOVA, $F(1, 17) = 0.1907$, $P$
809 $> 0.05$.

810 (H) Input–output curves of stimulus-evoked EPSPs from virgin mice (n = 9 cells; 5 animals) and
811 paternal mice (n = 10 cells; 4 animals) recorded with GDPβS (1 mM) in the pipette solution. Values
812 are presented as mean ± standard error. (inset) Representative traces used to construct

input–output curves (25, 75 and 125 μA stimuli). Two-way RM ANOVA, $F(1, 17) = 0.4811$, $P > 0.05$. (I) (top) Paired-pulse ratio of eEPSCs (inter-stimulation interval = 50 ms) from virgin mice (n = 6 cells; 5 animals) and paternal mice (n = 7 cells; 6 animals). Two-tailed unpaired t-test: $P > 0.05$. (bottom) Paired-pulse ratio of eIPSCs (inter-stimulation interval = 100 ms) from virgin mice (n = 10 cells; 9 animals) and paternal mice (n = 15 cells; 10 animals). Two-tailed unpaired t-test, $P > 0.05$.

## References


1. Elwood, R.W. (1977). Changes in Responses of Male and Female Gerbils (Meriones-Unguiculatus) Towards Test Pups during Pregnancy of Female. Anim Behav *25*, 46-51. Doi 10.1016/0003-3472(77)90066-5.
2. Hausfater, G., and Hrdy, S.B. (1984). Infanticide: Comparative and Evolutionary Perspectives (Routledge).
3. Hrdy, S.B. (1974). Male-Male Competition and Infanticide among Langurs (Presbytis-Entellus) of Abu, Rajasthan. Folia Primatol *22*, 19-58.
4. van Schaik, C.P., and Janson, C.P. (2000). Infanticide by Males and its Implications (Cambridge University Press).
5. vom Saal, F.S., and Howard, L.S. (1982). The regulation of infanticide and parental behavior: implications for reproductive success in male mice. Science *215*, 1270-1272.
6. Palombit, R.A. (2015). Infanticide as Sexual Conflict: Coevolution of Male Strategies and Female Counterstrategies. Csh Perspect Biol *7*. 10.1101/cshperspect.a017640.
7. vom Saal, F.S. (1985). Time-contingent change in infanticide and parental behavior induced by ejaculation in male mice. Physiol Behav *34*, 7-15.
8. Tachikawa, K.S., Yoshihara, Y., and Kuroda, K.O. (2013). Behavioral transition from attack to parenting in male mice: a crucial role of the vomeronasal system. The Journal of neuroscience : the official journal of the Society for Neuroscience *33*, 5120-5126. 10.1523/JNEUROSCI.2364-12.2013.
9. Numan, M. (1974). Medial preoptic area and maternal behavior in the female rat. J Comp Physiol Psychol *87*, 746-759.
10. Tsuneoka, Y., Maruyama, T., Yoshida, S., Nishimori, K., Kato, T., Numan, M., and Kuroda, K.O. (2013). Functional, anatomical, and neurochemical differentiation of medial preoptic area subregions in relation to maternal behavior in the mouse. The Journal of comparative

neurology *521*, 1633-1663. 10.1002/cne.23251.

11. Tsuneoka, Y., Tokita, K., Yoshihara, C., Amano, T., Esposito, G., Huang, A.J., Yu, L.M., Odaka, Y., Shinozuka, K., McHugh, T.J., and Kuroda, K.O. (2015). Distinct preoptic-BST nuclei dissociate paternal and infanticidal behavior in mice. The EMBO journal *34*, 2652-2670. 10.15252/embj.201591942.

12. Wu, Z., Autry, A.E., Bergan, J.F., Watabe-Uchida, M., and Dulac, C.G. (2014). Galanin neurons in the medial preoptic area govern parental behaviour. Nature *509*, 325-330. 10.1038/nature13307.

13. Keshavarzi, S., Sullivan, R.K., Ianno, D.J., and Sah, P. (2014). Functional properties and projections of neurons in the medial amygdala. The Journal of neuroscience : the official journal of the Society for Neuroscience *34*, 8699-8715. 10.1523/JNEUROSCI.1176-14.2014.

14. Kohl, J., Babayan, B.M., Rubinstein, N.D., Autry, A.E., Marin-Rodriguez, B., Kapoor, V., Miyamishi, K., Zweifel, L.S., Luo, L., Uchida, N., and Dulac, C. (2018). Functional circuit architecture underlying parental behaviour. Nature *556*, 326-331. 10.1038/s41586-018-0027-0.

15. Simerly, R.B., and Swanson, L.W. (1986). The organization of neural inputs to the medial preoptic nucleus of the rat. The Journal of comparative neurology *246*, 312-342. 10.1002/cne.902460304.

16. Mei, L., Yan, R., Yin, L., Sullivan, R.M., and Lin, D. (2023). Antagonistic circuits mediating infanticide and maternal care in female mice. Nature. 10.1038/s41586-023-06147-9.

17. Chen, P.B., Hu, R.K., Wu, Y.E., Pan, L., Huang, S., Micevych, P.E., and Hong, W. (2019). Sexually Dimorphic Control of Parenting Behavior by the Medial Amygdala. Cell *176*, 1206-1221.e1218. 10.1016/j.cell.2019.01.024.

18. Broberger, C. (1999). Hypothalamic cocaine- and amphetamine-regulated transcript (CART) neurons: histochemical relationship to thyrotropin-releasing hormone, melanin-concentrating hormone, orexin/hypocretin and neuropeptide Y. Brain Res *848*, 101-113.

19. Wu, Y.E., Pan, L., Zuo, Y., Li, X., and Hong, W. (2017). Detecting Activated Cell Populations Using Single-Cell RNA-Seq. Neuron *96*, 313-329 e316. 10.1016/j.neuron.2017.09.026.

20. Sato, K., Hamasaki, Y., Fukui, K., Ito, K., Miyamichi, K., Minami, M., and Amano, T. (2020). Amygdalohippocampal Area Neurons That Project to the Preoptic Area Mediate Infant-Directed Attack in Male Mice. The Journal of neuroscience : the official journal of the Society for Neuroscience *40*, 3981-3994. 10.1523/JNEUROSCI.0438-19.2020.

21. Moffitt, J.R., Bambah-Mukku, D., Eichhorn, S.W., Vaughn, E., Shekhar, K., Perez, J.D., Rubinstein, N.D., Hao, J., Regev, A., Dulac, C., and Zhuang, X. (2018). Molecular, spatial, and functional single-cell profiling of the hypothalamic preoptic region. Science *362*. 10.1126/science.aau5324.

22. Fang, Y.Y., Yamaguchi, T., Song, S.C., Tritsch, N.X., and Lin, D. (2018). A Hypothalamic

Midbrain Pathway Essential for Driving Maternal Behaviors. Neuron *98*, 192-207 e110. 10.1016/j.neuron.2018.02.019.

23. Wei, Y.C., Wang, S.R., Jiao, Z.L., Zhang, W., Lin, J.K., Li, X.Y., Li, S.S., Zhang, X., and Xu, X.H. (2018). Medial preoptic area in mice is capable of mediating sexually dimorphic behaviors regardless of gender. Nat Commun *9*, 279. 10.1038/s41467-017-02648-0.

24. Masseck, O.A., Spoida, K., Dalkara, D., Maejima, T., Rubelowski, J.M., Wallhorn, L., Deneris, E.S., and Herlitze, S. (2014). Vertebrate cone opsins enable sustained and highly sensitive rapid control of Gi/o signaling in anxiety circuitry. Neuron *81*, 1263-1273. 10.1016/j.neuron.2014.01.041.

25. Soya, S., Takahashi, T.M., McHugh, T.J., Maejima, T., Herlitze, S., Abe, M., Sakimura, K., and Sakurai, T. (2017). Orexin modulates behavioral fear expression through the locus coeruleus. Nat Commun *8*, 1606. 10.1038/s41467-017-01782-z.

26. Amano, T., Shindo, S., Yoshihara, C., Tsuneoka, Y., Uki, H., Minami, M., and Kuroda, K.O. (2017). Development-dependent behavioral change toward pups and synaptic transmission in the rhomboid nucleus of the bed nucleus of the stria terminalis. Behav Brain Res *325*, 131-137. 10.1016/j.bbr.2016.10.029.

27. Elwood, R.W. (1985). Inhibition of Infanticide and Onset of Paternal Care in Male-Mice (Mus-Musculus). J Comp Psychol *99*, 457-467. Doi 10.1037//0735-7036.99.4.457.

28. Inada, K., Hagihara, M., Tsujimoto, K., Abe, T., Konno, A., Hirai, H., Kiyonari, H., and Miyamichi, K. (2022). Plasticity of neural connections underlying oxytocin-mediated parental behaviors of male mice. Neuron. 10.1016/j.neuron.2022.03.033.

29. Hong, W., Kim, D.W., and Anderson, D.J. (2014). Antagonistic control of social versus repetitive self-grooming behaviors by separable amygdala neuronal subsets. Cell *158*, 1348-1361. 10.1016/j.cell.2014.07.049.

30. Kondo, Y. (1992). Lesions of the medial amygdala produce severe impairment of copulatory behavior in sexually inexperienced male rats. Physiol Behav *51*, 939-943.

31. Li, Y., Mathis, A., Grewe, B.F., Osterhout, J.A., Ahanonu, B., Schnitzer, M.J., Murthy, V.N., and Dulac, C. (2017). Neuronal Representation of Social Information in the Medial Amygdala of Awake Behaving Mice. Cell *171*, 1176-1190 e1117. 10.1016/j.cell.2017.10.015.

32. Sano, K., Nakata, M., Musatov, S., Morishita, M., Sakamoto, T., Tsukahara, S., and Ogawa, S. (2016). Pubertal activation of estrogen receptor alpha in the medial amygdala is essential for the full expression of male social behavior in mice. Proc Natl Acad Sci U S A *113*, 7632-7637. 10.1073/pnas.1524907113.

33. Sano, K., Tsuda, M.C., Musatov, S., Sakamoto, T., and Ogawa, S. (2013). Differential effects of site-specific knockdown of estrogen receptor alpha in the medial amygdala, medial pre-optic area, and ventromedial nucleus of the hypothalamus on sexual and aggressive behavior of male mice. Eur J Neurosci *37*, 1308-1319. 10.1111/ejn.12131.

34. Dominguez, J., Riolo, J.V., Xu, Z., and Hull, E.M. (2001). Regulation by the medial

amygdala of copulation and medial preoptic dopamine release. The Journal of neuroscience : the official journal of the Society for Neuroscience *21*, 349-355.

35. Kondo, Y., and Arai, Y. (1995). Functional association between the medial amygdala and the medial preoptic area in regulation of mating behavior in the male rat. Physiol Behav *57*, 69-73.

36. Choi, G.B., Dong, H.W., Murphy, A.J., Valenzuela, D.M., Yancopoulos, G.D., Swanson, L.W., and Anderson, D.J. (2005). Lhx6 delineates a pathway mediating innate reproductive behaviors from the amygdala to the hypothalamus. Neuron *46*, 647-660. 10.1016/j.neuron.2005.04.011.

37. Pardo-Bellver, C., Cadiz-Moretti, B., Novejarque, A., Martinez-Garcia, F., and Lanuza, E. (2012). Differential efferent projections of the anterior, posteroventral, and posterodorsal subdivisions of the medial amygdala in mice. Front Neuroanat *6*, 33. 10.3389/fnana.2012.00033.

38. Morris, J.A., Jordan, C.L., and Breedlove, S.M. (2008). Sexual dimorphism in neuronal number of the posterodorsal medial amygdala is independent of circulating androgens and regional volume in adult rats. The Journal of comparative neurology *506*, 851-859. 10.1002/cne.21536.

39. Unger, E.K., Burke, K.J., Jr., Yang, C.F., Bender, K.J., Fuller, P.M., and Shah, N.M. (2015). Medial amygdalar aromatase neurons regulate aggression in both sexes. Cell Rep *10*, 453-462. 10.1016/j.celrep.2014.12.040.

40. Rogge, G., Jones, D., Hubert, G.W., Lin, Y., and Kuhar, M.J. (2008). CART peptides: regulators of body weight, reward and other functions. Nat Rev Neurosci *9*, 747-758. 10.1038/nrn2493.

41. Allen, W.E., DeNardo, L.A., Chen, M.Z., Liu, C.D., Loh, K.M., Fenno, L.E., Ramakrishnan, C., Deisseroth, K., and Luo, L. (2017). Thirst-associated preoptic neurons encode an aversive motivational drive. Science *357*, 1149-1155. 10.1126/science.aan6747.

42. Chung, S., Weber, F., Zhong, P., Tan, C.L., Nguyen, T.N., Beier, K.T., Hormann, N., Chang, W.C., Zhang, Z., Do, J.P., et al. (2017). Identification of preoptic sleep neurons using retrograde labelling and gene profiling. Nature *545*, 477-481. 10.1038/nature22350.

43. McHenry, J.A., Otis, J.M., Rossi, M.A., Robinson, J.E., Kosyk, O., Miller, N.W., McElligott, Z.A., Budygin, E.A., Rubinow, D.R., and Stuber, G.D. (2017). Hormonal gain control of a medial preoptic area social reward circuit. Nat Neurosci *20*, 449-458. 10.1038/nn.4487.

44. Tan, C.L., Cooke, E.K., Leib, D.E., Lin, Y.C., Daly, G.E., Zimmerman, C.A., and Knight, Z.A. (2016). Warm-Sensitive Neurons that Control Body Temperature. Cell *167*, 47-59 e15. 10.1016/j.cell.2016.08.028.

45. Fumero, B., Fernandez-Vera, J.R., Gonzalez-Mora, J.L., and Mas, M. (1994). Changes in monoamine turnover in forebrain areas associated with masculine sexual behavior: a

958 microdialysis study. Brain Res *662*, 233-239.
959 46. Nutsch, V.L., Will, R.G., Robison, C.L., Martz, J.R., Tobiansky, D.J., and Dominguez, J.M.
960 (2016). Colocalization of Mating-Induced Fos and D2-Like Dopamine Receptors in the Medial
961 Preoptic Area: Influence of Sexual Experience. Front Behav Neurosci *10*, 75.
962 10.3389/fnbeh.2016.00075.
963 47. Ren, W.J., Centeno, M.V., Berger, S., Wu, Y., Na, X.D., Liu, X.G., Kondapalli, J.,
964 Apkarian, A.V., Martina, M., and Surmeier, D.J. (2016). The indirect pathway of the
965 nucleus accumbens shell amplifies neuropathic pain. Nature Neuroscience *19*, 220-+.
966 10.1038/nn.4199.
967 48. Thompson, D., Martini, L., and Whistler, J.L. (2010). Altered ratio of D1 and D2 dopamine
968 receptors in mouse striatum is associated with behavioral sensitization to cocaine. PLoS
969 One *5*, e11038. 10.1371/journal.pone.0011038.
970 49. Jacob, T.C., Moss, S.J., and Jurd, R. (2008). GABA(A) receptor trafficking and its role in
971 the dynamic modulation of neuronal inhibition. Nat Rev Neurosci *9*, 331-343.
972 10.1038/nrn2370.
973 50. Seelke, A.M.H., Bond, J.M., Simmons, T.C., Joshi, N., Settles, M.L., Stolzenberg, D.,
974 Rhemtulla, M., and Bales, K.L. (2018). Fatherhood alters gene expression within the MPOA.
975 Environ Epigenet *4*, dvy026. 10.1093/eep/dvy026.
976 51. Tsuneoka, Y., Yoshida, S., Takase, K., Oda, S., Kuroda, M., and Funato, H. (2017).
977 Neurotransmitters and neuropeptides in gonadal steroid receptor-expressing cells in medial
978 preoptic area subregions of the male mouse. Sci Rep *7*, 9809. 10.1038/s41598-017-10213-4.
979 52. Kawai, S., Takagi, Y., Kaneko, S., and Kurosawa, T. (2011). Effect of three types of mixed
980 anesthetic agents alternate to ketamine in mice. Exp Anim *60*, 481-487.
981 53. Tsuneoka, Y., Atsumi, Y., Makanae, A., Yashiro, M., and Funato, H. (2022). Fluorescence
982 quenching by high-power LEDs for highly sensitive fluorescence in situ hybridization.
983 Front Mol Neurosci *15*, 976349. 10.3389/fnmol.2022.976349.
984 54. Tsuneoka, Y., and Funato, H. (2020). Modified in situ Hybridization Chain Reaction Using
985 Short Hairpin DNAs. Front Mol Neurosci *13*, 75. 10.3389/fnmol.2020.00075.
986 55. Picelli, S., Faridani, O.R., Bjorklund, A.K., Winberg, G., Sagasser, S., and Sandberg, R.
987 (2014). Full-length RNA-seq from single cells using Smart-seq2. Nat Protoc *9*, 171-181.
988 10.1038/nprot.2014.006.
989 56. Dobin, A., Davis, C.A., Schlesinger, F., Drenkow, J., Zaleski, C., Jha, S., Batut, P.,
990 Chaisson, M., and Gingeras, T.R. (2013). STAR: ultrafast universal RNA-seq aligner.
991 Bioinformatics *29*, 15-21. 10.1093/bioinformatics/bts635.

992

Figure 1

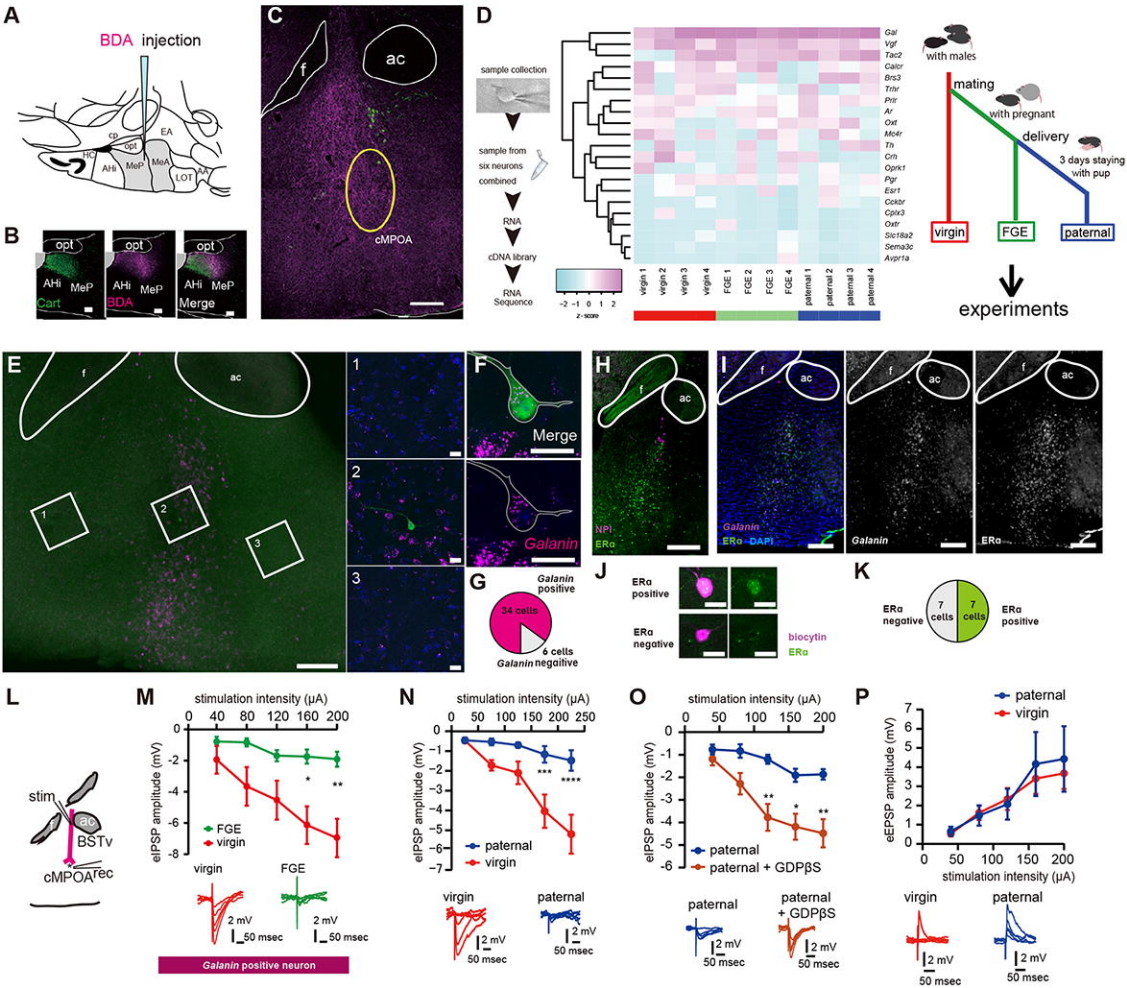
A
BDA injection
cp
opt
EA
HC
AHi
MeP
MeA
LOT
APir
B
opt
AHi
MeP
Cart
BDA
Merge
C
f
ac
cMPOA
D
sample collection
sample from six neurons combined
RNA
cDNA library
RNA Sequence
Gal
Vgf
Tac2
Calcr
Brs3
Trhr
Prlr
Ar
Oxt
Mc4r
Th
Crh
Oprk1
Pgr
Esr1
Cckbr
Cplx3
Oxtr
Slc18a2
Sema3c
Avpr1a
virgin 1
virgin 2
virgin 3
virgin 4
FGE 1
FGE 2
FGE 3
FGE 4
paternal 1
paternal 2
paternal 3
paternal 4
z-score
with males
mating
with pregnant
delivery
3 days staying with pup
virgin
FGE
paternal
experiments
E
f
ac
1
2
3
F
Merge
Galanin
G
Galanin positive
34 cells
6 cells
Galanin negative
H
f
ac
NPi
ERα
I
f
ac
Galanin
ERα
DAPI
ERα
J
ERα positive
ERα negative
biocytin
ERα
K
ERα negative
7 cells
7 cells
ERα positive
L
stim
ac
BSTv
cMPOA
rec
M
stimulation intensity (μA)
eIPSP amplitude (mV)
FGE
virgin
virgin
FGE
2 mV
50 msec
Galanin positive neuron
N
stimulation intensity (μA)
eIPSP amplitude (mV)
paternal
virgin
virgin
paternal
O
stimulation intensity (μA)
eIPSP amplitude (mV)
paternal
paternal + GDPβS
paternal
paternal + GDPβS
P
paternal
virgin
eEPSP amplitude (mV)
stimulation intensity (μA)
virgin
paternal

Figure 2

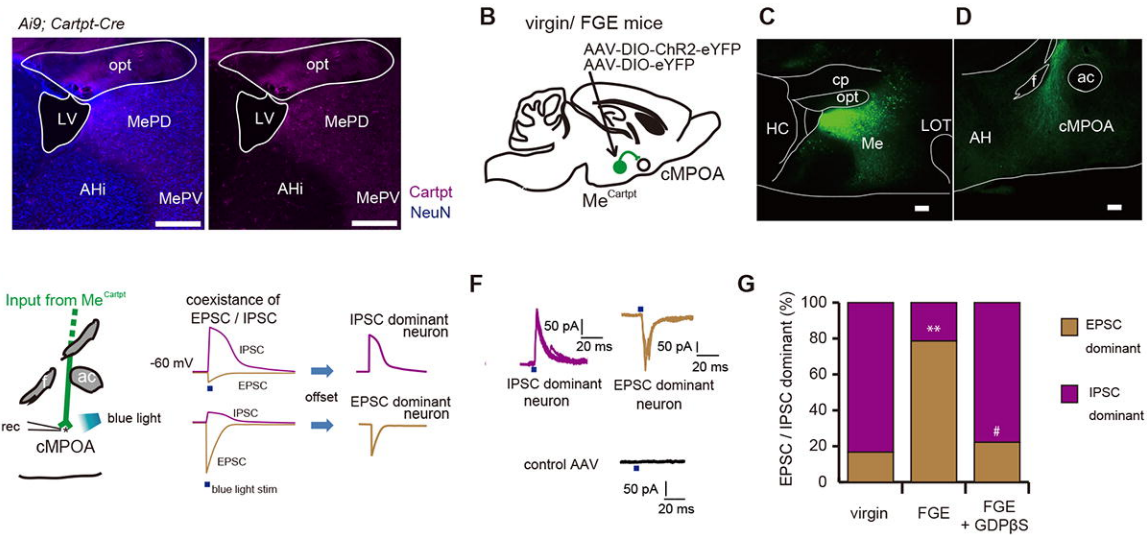
A
Ai9; Cartpt-Cre
opt
LV
MePD
AHi
MePV
Cartpt
NeuN
B
virgin/ FGE mice
AAV-DIO-ChR2-eYFP
AAV-DIO-eYFP
cMPOA
Me Cartpt
C
cp
opt
HC
Me
LOT
D
f
ac
AH
cMPOA
E
Input from Me Cartpt
ac
rec
blue light
cMPOA
coexistance of
EPSC / IPSC
-60 mV
IPSC
EPSC
IPSC dominant
neuron
offset
EPSC dominant
neuron
blue light stim
F
50 pA
20 ms
IPSC dominant
neuron
EPSC dominant
neuron
control AAV
G
EPSC / IPSC dominant (%)
100
80
60
40
20
0
**
#
virgin
FGE
FGE
+ GDPβS
EPSC
dominant
IPSC
dominant

Figure 3

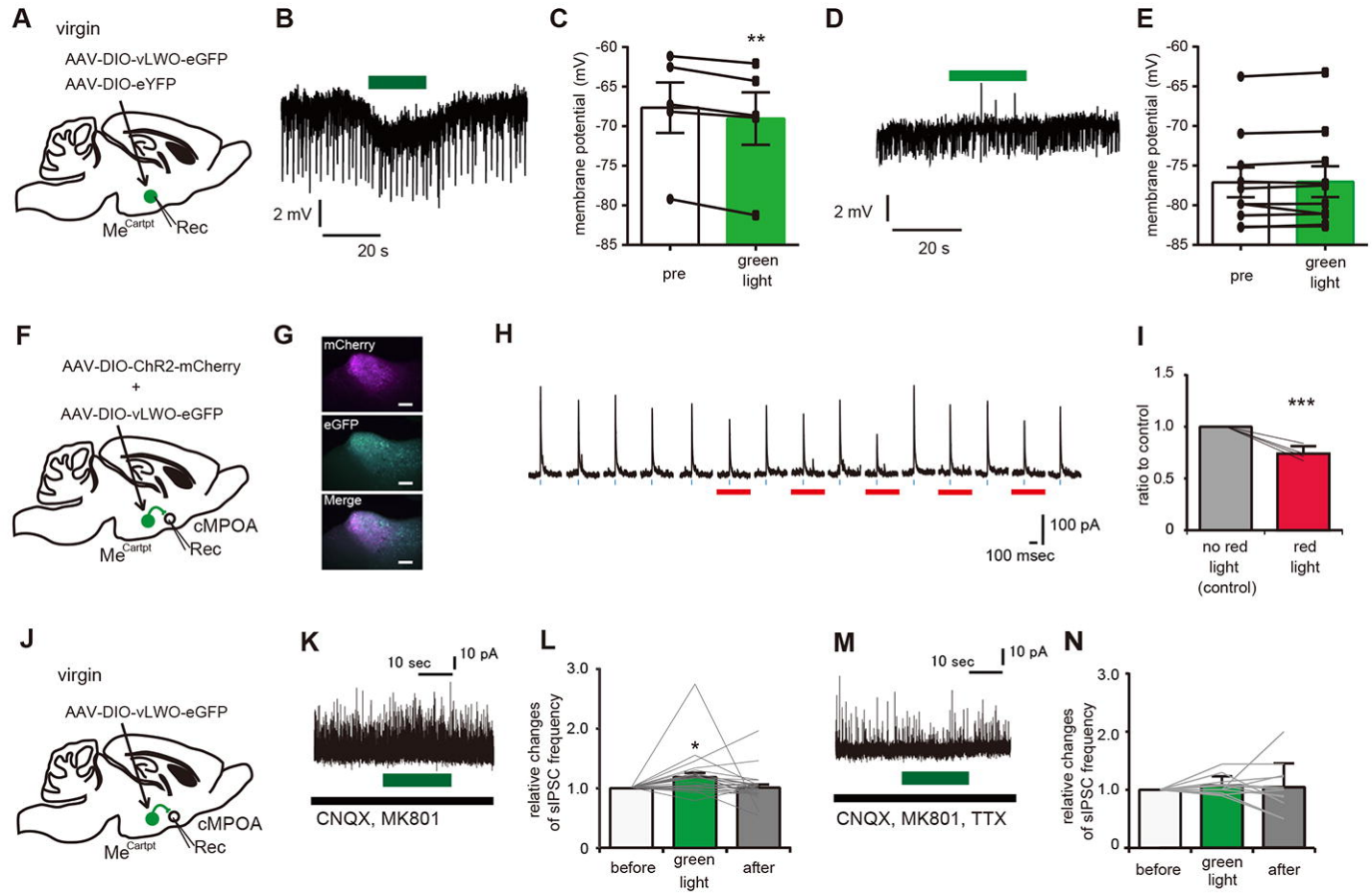
A
virgin
AAV-DIO-vLWO-eGFP
AAV-DIO-eYFP
Me Cartpt
Rec
B
2 mV
20 s
C
membrane potential (mV)
-60
-65
-70
-75
-80
-85
**
pre
green light
D
2 mV
20 s
E
membrane potential (mV)
-60
-65
-70
-75
-80
-85
pre
green light
F
AAV-DIO-ChR2-mCherry
+
AAV-DIO-vLWO-eGFP
cMPOA
Me Cartpt
Rec
G
mCherry
eGFP
Merge
H
100 pA
100 msec
I
ratio to control
1.5
1.0
0.5
0
***
no red light (control)
red light
J
virgin
AAV-DIO-vLWO-eGFP
cMPOA
Me Cartpt
Rec
K
10 sec
10 pA
CNQX, MK801
L
relative changes of sIPSC frequency
3.0
2.0
1.0
0
*
before
green light
after
M
10 sec
10 pA
CNQX, MK801, TTX
N
relative changes of sIPSC frequency
3.0
2.0
1.0
0
before
green light
after

Figure 4

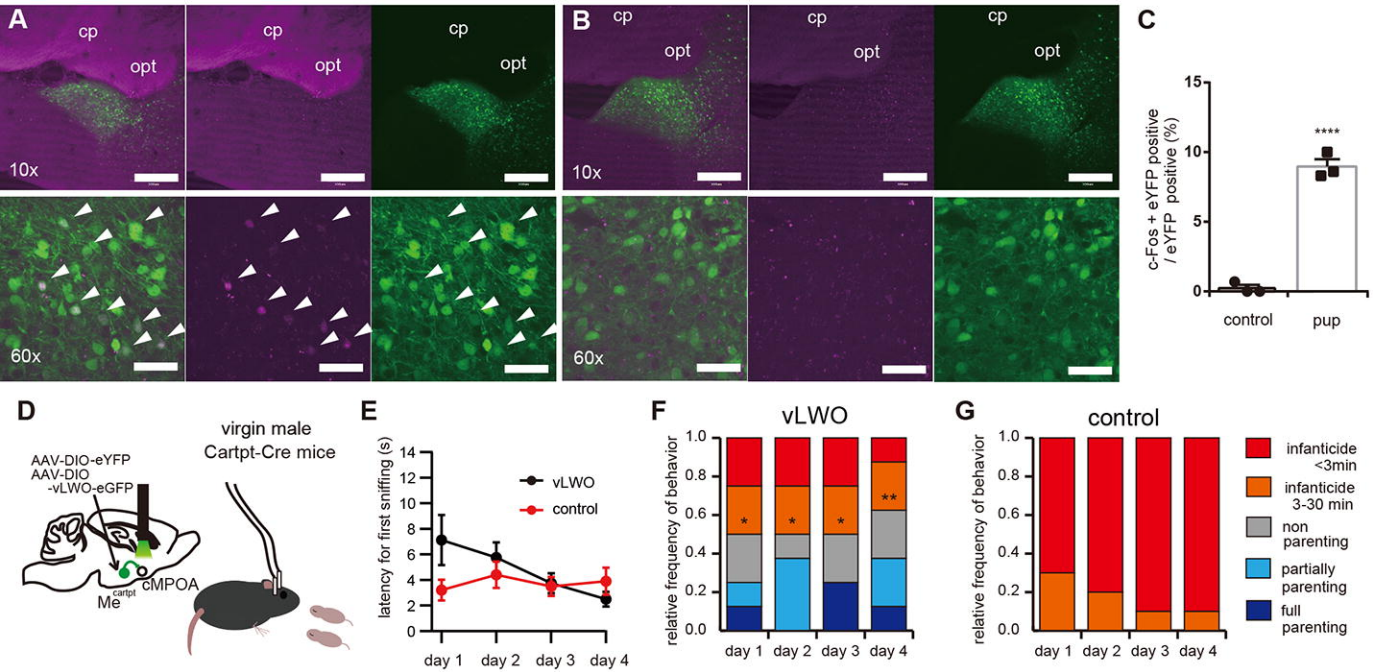
A
cp
opt
10x
60x
B
C
c-Fos + eYFP positive / eYFP positive (%)
****
control
pup
D
virgin male
Cartpt-Cre mice
AAV-DIO-eYFP
AAV-DIO
-vLWO-eGFP
cMPOA
Me
cartpt
E
latency for first sniffing (s)
vLWO
control
day 1
day 2
day 3
day 4
F
vLWO
relative frequency of behavior
G
control
infanticide <3min
infanticide 3-30 min
non parenting
partially parenting
full parenting

# Figure 5

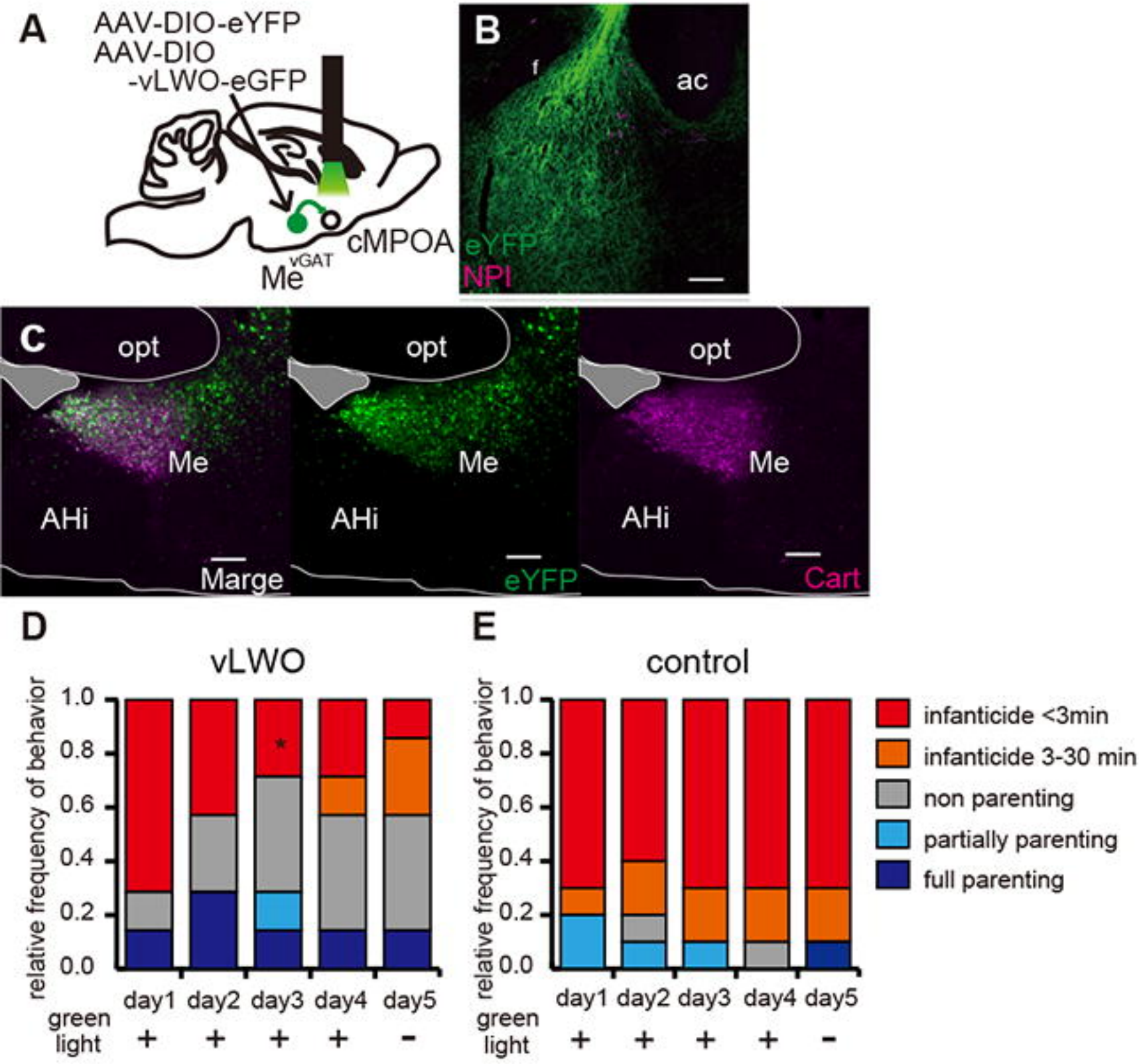
A
AAV-DIO-eYFP
AAV-DIO
-vLWO-eGFP
cMPOA
Me
vGAT
B
f
ac
eYFP
NPI
C
opt
Me
AHi
Marge
eYFP
Cart
D
vLWO
relative frequency of behavior
1.0
0.8
0.6
0.4
0.2
0.0
day1 day2 day3 day4 day5
green light
+ + + + -
E
control
relative frequency of behavior
day1 day2 day3 day4 day5
green light
+ + + + -
infanticide <3min
infanticide 3-30 min
non parenting
partially parenting
full parenting

Figure 6

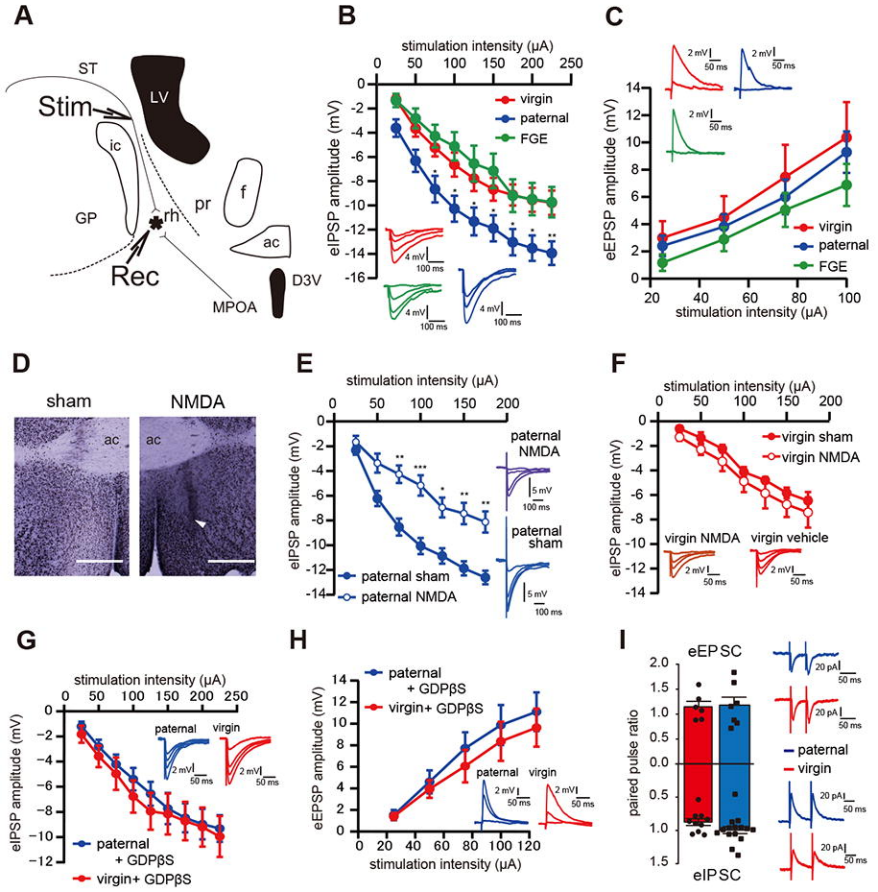
A
ST
LV
Stim
ic
GP
rh
pr
f
ac
Rec
D3V
MPOA
B
stimulation intensity (μA)
eIPSP amplitude (mV)
virgin
paternal
FGE
C
eEPSP amplitude (mV)
stimulation intensity (μA)
virgin
paternal
FGE
D
sham
NMDA
ac
ac
E
stimulation intensity (μA)
eIPSP amplitude (mV)
paternal NMDA
paternal sham
F
stimulation intensity (μA)
eIPSP amplitude (mV)
virgin sham
virgin NMDA
virgin NMDA
virgin vehicle
G
stimulation intensity (μA)
eIPSP amplitude (mV)
paternal
virgin
paternal + GDPβS
virgin+ GDPβS
H
paternal + GDPβS
virgin+ GDPβS
eEPSP amplitude (mV)
paternal
virgin
stimulation intensity (μA)
I
eEPSC
paired pulse ratio
paternal
virgin
eIPSC

Graphical Abstract